FRACTURE AND FATIGUE CRACK GROWTH BEHAVIOUR OF ADDITIVELY MANUFACTURED MATERIAL

Thesis is submitted in partial fulfilment of the requirement for the degree of

MASTER OF MECHANICAL ENGINEERING

By:

SAGNIK GHATAK

Examination Roll No.: **M4MEC24002**

Registration No.: **163703** of **2022-2023**

Under the guidance of:

Dr. Anirban Mitra

Department of Mechanical Engineering

Faculty of Engineering and Technology

Jadavpur University

Kolkata-700032

August, 2024

FACULTY OF ENGINEERING AND TECHNOLOGY

JADAVPUR UNIVERSITY

KOLKATA – 700032

CERTIFICATE OF APPROVAL*

This forgiving thesis is air by approved as a credible study of an engineering subject carried out and presented in a manner satisfactory to warrant its acceptance as a prerequisite to the degree for which it has been submitted. It is understood that by this approval the undersigned do not endorse or approve any statement made, opinion expressed or concussion drawn therein but approved the thesis only for the purpose for which it has been submitted.

Committee
On Final Examination for
Evaluation of the Thesis

Signature: _____
Date: _____
Seal:

Signature: _____
Date: _____
Seal:

*** Only in case the thesis is approved**

FACULTY OF ENGINEERING AND TECHNOLOGY

JADAVPUR UNIVERSITY

KOLKATA – 700032

CERTIFICATE OF SUPERVISION

We hereby recommend that the thesis presented by Mr. SAGNIK GHATAK entitled **"FRACTURE AND FATIGUE CRACK GROWTH BEHAVIOUR OF ADDITIVELY MANUFACTURED MATERIAL"** was under our supervision and is accepted in partial fulfilment of the degree of Master of Mechanical Engineering.

_____

(Thesis Adviser)

Date: _____

Seal:

Countersigned by:

_____

(Head of the Department, Mechanical Engineering)

Date: _____

Seal:

_____

(Dean of Faculty of Engineering and Technology)

Date: _____

Seal:

FACULTY OF ENGINEERING AND TECHNOLOGY

DEPARTMENT OF MECHANICAL ENGINEERING

JADAVPUR UNIVERSITY

KOLKATA -700032

DECLARATION OF ORIGINALITY AND COMPLIANCE OF ACADEMIC ETHICS

I hereby declare that this thesis contains literature survey and original research work by the undersigned candidate, as part of his Master of mechanical engineering (Machine Design) studies.

All information in this document have been obtained and presented accordance with academic rules and ethical conduct.

I also declare that, as required by these rules and conduct, I have fully cited and referred all material and results that are not original to this work.

Name: Sagnik Ghatak

Examination Roll Number: M4MEC24002

Registration Number: 163703 of 2022-2023

Thesis Title:

_____

Signature:

(Sagnik Ghatak)

Dated:

Acknowledgements

I am deeply grateful to all those who have supported and guided me throughout my thesis work. First and foremost, I would like to express my sincere thanks to my supervisor, **Dr. Anirban Mitra**, for his steadfast support, patience, and invaluable technical discussions. His guidance has been a constant source of motivation and inspiration.

I am also indebted to my mentors, **Dr. Sanjib Kumar Acharyya** for his continuous support and insightful feedback. His expertise and encouragement have been instrumental in the successful completion of this work.

Special thanks are due to my seniors, **Md. Rakim**, **Dr. Debiprasanna Mohanty**, **Rakesh Bhadra**, **Manik Barman**, **Morsalim Mallick**, whose cooperation, goodwill, and technical advice were crucial in bringing this thesis to its final form. I am also thankful to **Shubhojit Ghosh** and **Sukamal Samanta** for their assistance and cooperation throughout this journey.

I would like to extend my appreciation to the faculty and staff of the **Mechanical Engineering Department** for providing a conducive environment for my research and study.

Lastly, I am profoundly grateful to **my Parents** for their unwavering faith, unconditional love, and constant support. Their encouragement and patience have been my greatest strength.

Date: SAGNIK GHATAK

Abstract

This thesis explores the fracture and fatigue crack growth behaviour of 3D-printed Polylactic Acid (PLA) specimens produced via Fused Deposition Modelling (FDM). As additive manufacturing (AM) advances, understanding the mechanical reliability of printed components under cyclic loading and fracture conditions is critical yet under-researched. The study investigates the impact of varying infill densities of 25%, 50%, and 100% with a honeycomb infill pattern on the tensile properties, fatigue crack growth rate (FCGR) and fracture toughness of PLA specimens. Mechanical testing, conducted according to ASTM standards, reveals significant correlations between infill density and mechanical performance. Higher infill densities result in increased tensile strength, enhanced fracture resistance, and distinct fatigue behaviour, emphasizing the influence of the internal structure on material properties. The findings provide essential insights into optimizing FDM processes for critical applications, addressing the research gap in the mechanical characterization of AM materials. This work contributes to the broader application of FDM-printed PLA in industries requiring reliable performance under diverse loading conditions, such as aerospace, biomedical, and automotive engineering.

Table of Contents

List of Figures:

List of Tables

Chapter 1: Introduction

1.1 Introduction

Additive manufacturing promises a new industrial revolution by enabling the production of parts through the repetitive layer-wise deposition of material from a digital CAD model. Various techniques have been developed, allowing for the creation of complex geometries and fabrication of components utilising functionally graded materials. Such complexity in terms of geometries and scope of use of advanced materials are not available with traditional methods. This flexibility in design paves the way for new engineering paradigms and offers benefits such as repairing expensive parts, manufacturing in remote locations, and producing customized parts on demand.

However, to fully leverage these capabilities, the structural integrity of additively manufactured parts must be understood and characterized. Despite the potential for creating geometrically complex parts using topological optimization, the mechanical behaviour and reliability of these parts are not yet fully documented, hindering widespread adoption in industries such as aerospace, biomedical, and automotive.

The fracture parameters and fatigue resistance of additively manufactured parts can differ from traditionally manufactured ones due to the localized heating and cooling processes, varying powder quality, and high cooling rates, leading to unique microstructures with significant anisotropy. Additionally, severe thermal gradients can cause residual stresses and distortion. Interactions between the powder and heat source, along with the layer-by-layer process, can lead to defects such as porosity and lack of fusion, which may initiate fatigue cracks. Establishing process–structure relationships for additive manufacturing is essential. An additively manufactured component may inherently have structured porosity in its interior due understood thoroughly.

There are many different additive manufacturing techniques such as material extrusion, powder bed fusion, directed energy deposition, vat polymerization, binder jetting and each have their own parameters and characteristics. A fundamental understanding and establishment of process-structure relationship for additive manufacturing is essential.

1.2. Literature Review

A literature survey is always a good starting point for any research work as it provides a clear picture and understanding of the present-state-of-the-art. Review of literature on additive manufacturing (AM) reveals significant advancements in material properties, including fatigue crack growth rate and fracture toughness. Research highlights the impact of AM techniques, such as fused deposition modelling on enhancing these properties. Studies show that AM materials exhibit unique microstructures, influencing their mechanical performance under cyclic loading and fracture conditions. Understanding these aspects is crucial for optimizing AM processes and ensuring the reliability of components in critical applications. The present survey synthesizes findings from various studies, providing insights into the interplay between AM methods and material characteristics, properties and durability. The literature review offers a thorough analysis of the mechanical attributes of additively manufactured materials, particularly focusing on tensile properties, fatigue-fracture behaviour, and the challenges in achieving consistent outcomes. The emphasis on Polylactic Acid (PLA) stems from its prominence in FDM 3D printing, its biodegradability, and its suitability for diverse applications. The thesis experimentally investigates the impact of infill density on the tensile properties, fatigue crack growth rate, and fracture toughness of 3D-printed PLA using the FDM technique. The findings contribute to optimizing the design and fabrication of 3D-printed PLA components, advancing the field of additive manufacturing.

The thesis covers the following key points:

- Fabrication of FDM-printed PLA specimens adhering to ASTM standards.

- Tensile testing to analyse the effect of infill density on mechanical properties.
- FCGR testing to determine fatigue behaviour parameters.
- Fracture toughness testing to assess the impact of infill density on fracture resistance.

The choice of PLA is attributed to its widespread use in FDM 3D printing, its biodegradability, and its potential for various applications, making it a relevant and practical material for investigation in the context of additive manufacturing.

1.2.1 Literature Review on Tensile properties of Additively Manufactured materials:

Ngo et al., [1] reviewed additive manufacturing (AM) or 3D printing methods, materials, and applications. The authors discussed the advantages of AM, such as freedom of design, customization, and waste minimization, as well as its applications in various fields, including biomedical, aerospace, construction, and protective structures. The review also addressed the challenges of AM, such as void formation, anisotropic behaviour, and limitations in materials and design tools.

Shanmugam et al., [2] reviewed the mechanical testing and performance analysis of polymer-fibre composites fabricated through additive manufacturing, specifically fused deposition modelling (FDM). The review highlights the impact of various FDM processing parameters on the mechanical properties of these composites. Additionally, the review briefly discussed the thermal properties of FDM-based fibre composites. The authors emphasize that the bonding between layers, fibre-matrix characteristics, fibre-matrix interface, and FDM printing variables all play a crucial role in the mechanical and thermal performance of the final composite product.

Doshi et al., [3] analysed how printing parameters affect the mechanical properties of components manufactured using fused deposition modelling (FDM), emphasizing tensile strength, stress, and Young's modulus. Key parameters included layer thickness, build

orientation, printing speed, infill density, printing speed, infill pattern and raster angle. Findings indicate that PLA and ABS were the most used materials, with optimal properties achieved at 100% infill density for highest Young's modulus, 90 mm/s infill speed for best layer structure, and 215°C for PLA filament. Orientation and raster angle significantly influenced tensile strength, with a 0° raster angle yielding the best results.

Samykano et al., [4] Explored how three printing parameters such as infill density, layer height, and raster angle affect the mechanical properties (ultimate tensile strength, yield strength, elastic modulus, toughness, and fracture strain) of 3D-printed ABS components produced by fused deposition modelling (FDM). The findings indicated that infill density had the greatest impact on these properties. The optimal 3D printing settings for ABS were identified as 80% infill density, 0.5 mm layer thickness, and a 65° raster angle. Additionally, a mathematical model was created using response surface methodology to predict the tensile properties of ABS based on these printing parameters.

Dawoud et al., [5] compared the mechanical behaviour of ABS parts produced by fused deposition modelling (FDM) and injection moulding. The study investigated the effect of FDM parameters (raster angle and gap) on tensile, flexural, and impact strength. The results showed that FDM parts with negative raster gaps achieved 98% of the density of injection moulded parts. A negative raster gap and 45° raster angle resulted in the highest tensile and impact strength for FDM parts, while a 0° raster angle yielded the highest flexural strength. The study concluded that with proper parameter selection, FDM can produce parts with comparable mechanical properties to injection moulding.

Uddin et al., [6] investigated the influence of printing parameters (layer thickness, printing plane, and printing orientation) on the mechanical properties (Young's modulus, yield strength, failure strength, and strain) of 3D printed ABS parts using FDM and compared them to injection-moulded ABS parts. The results showed that the tensile properties of the printed

parts were highly dependent on the printing parameters, with the YZ-H orientation and 0.09 mm layer thickness exhibiting the highest stiffness and failure strength. While injection-moulded specimens showed the highest yield strength, printed specimens demonstrated greater ductility. The study also revealed that the failure mechanisms of printed parts varied depending on the printing parameters and loading conditions (tensile or compressive).

Vikneswaran et al., [7] studied the tensile behaviour of PLA, ABS, and PETG materials used in FDM 3D printing. The authors 3D printed tensile specimens according to ASTM standards and tested them using a universal testing machine. The results showed that PETG had the highest elongation and tensile strength, while ABS had the highest stiffness. PLA had a tensile strength similar to PETG but was less ductile. The authors concluded that PETG is suitable for applications requiring high tensile strength, while PLA is suitable for applications requiring minimal elongation and medium tensile strength.

Riddick et al., [8] investigated the effects of build direction (horizontal, side, vertical) and raster orientation (±45°, 0°, 90°, 0°/90°) on the tensile properties and failure mechanisms of ABS specimens fabricated using fused deposition modelling (FDM). The study found that the specimens exhibited anisotropic mechanical behaviour, with the side build direction generally showing the highest tensile strength and modulus for all raster orientations. The fracture surfaces were analysed using scanning electron microscopy, revealing different failure modes depending on the build direction and raster orientation. The authors concluded that the mechanical properties and failure mechanisms of FDM-fabricated ABS parts are highly dependent on the printing parameters, and this knowledge can be used to optimize the design and fabrication of complex lightweight structures.

Musa et al., [9] reviewed the potential of thermoplastic elastomers (TPEs) as filament material for fused deposition modelling (FDM) 3D printing. TPEs are a blend of a thermoplastic, such as polylactic acid (PLA), and an elastomer, such as natural rubber (NR).

The authors highlighted that TPEs offer the flexibility and renewability of elastomers while maintaining the thermoplastic-like processability of PLA. The resulting printed components are flexible, tough, and exhibit excellent thermal and mechanical properties, making TPE blends a promising filament material for FDM.

Prajapati et al., [10] reviewed the physical and mechanical properties of PLA, ABS, TPU, and PETG materials used in fused deposition modelling (FDM) 3D printing. The study focused on mechanical properties such as density, tensile strength, and flexural strength. The authors found that the mechanical properties of these materials vary depending on the printing parameters and post-processing techniques. The review also highlighted the need for further research to optimize the FDM process for achieving desired material properties in 3D printed components.

Raney et al., [11] experimentally characterized the tensile strength of ABS parts manufactured using fused deposition modelling (FDM). The study investigated the effects of specimen orientation (flat, horizontal, vertical) and infill percentage (low, high, solid) on tensile strength, yield strength, strain, and Young's modulus. The results showed that the solid infill group had the highest tensile strength, while the vertical orientation had the lowest. The study also found that the bonds between layers were weaker than the axial loading along the layers, highlighting the anisotropic behaviour of FDM-printed parts.

Arjun et al., [12] investigated the effects of process parameters (infill density, infill pattern, nozzle temperature, layer height, and print speed) and thermal annealing on the tensile strength of 3D printed carbon fibre reinforced polylactic acid (PLA) using fused filament fabrication (FFF). The study found that the optimal process parameters for maximum tensile strength were 90% infill density, gyroid infill pattern, 230^0 C nozzle temperature, 0.1 mm layer height, and 40 mm/s print speed. Additionally, annealing at 95^0 C for 120 minutes further increased the tensile strength by 14%. The authors concluded that optimizing process

parameters and post-processing techniques can significantly improve the mechanical properties of FFF 3D printed composites.

Mallikarjuna et al., [13] investigated the effects of infill density (20%, 25%, 30%), print temperature (225^0, 235^0, 245^0C), and print speed (20, 25, 30 mm/s) on the mechanical properties of PETG parts produced using FDM. The study found that samples with 25% infill density exhibited higher tensile, flexural, and impact strengths. The highest ultimate tensile strength (35.46 MPa) was achieved with 30% infill density, 245^0C extrusion temperature, and 25 mm/s print speed. Compression strength was directly proportional to infill density, and impact strength was highest for samples printed at 25 mm/s.

Shashikumar et al., [14] evaluated the influence of raster orientation ($0, +45/-45, 90\ and\ 0/90\ degrees$) and layer thickness ($0.1, 0.2, 0.3, and\ 0.4\ mm$) on the tensile properties of 3D printed ABS (amorphous) and Nylon 6 (semi-crystalline) using FDM. A 90-degree raster orientation and a 0.1 mm layer thickness produced the highest ultimate tensile strength (UTS) for both materials. However, at greater layer thicknesses (0.3-0.4 mm), the +45/-45 degree raster angle achieved the highest UTS. Nylon 6 demonstrated greater tensile toughness and elongation than ABS.

Zhang et al., [15] conducted a systematic investigation on the minimum tensile strengths and size effects of four common 3D printing polymers (ABS, PLA, PC, and PA12) fabricated by fused deposition modelling (FDM) and injection moulding. The study found that the minimum tensile strengths were in the build direction (perpendicular to the printing surface) and could be as low as 25% of the strengths in other directions. The size effect was significant for PLA and PC specimens printed along the build direction, with strengths decreasing up to 72% as the cross-sectional area increased 60 times.

Rodríguez-Panes et al., [16] compared the tensile mechanical behaviour of 3D printed parts made from PLA and ABS using FDM. The study investigated the effects of layer height,

infill density, and layer orientation on tensile yield stress, tensile strength, nominal strain at break, and modulus of elasticity. The results showed that ABS had lower variability in mechanical properties than PLA. PLA exhibited higher rigidity and tensile strength, while ABS was more ductile. Infill percentage was the most influential parameter, especially for PLA. The study also found that the bond between layers was stronger in PLA, making it more suitable for FDM.

Akhoundi et al., [17] experimentally investigated the effect of filling pattern (concentric, rectilinear, Hilbert curve, and honeycomb) and infill percentage (20%, 50%, and 100%) on the tensile and flexural properties of FDM 3D printed parts. The concentric pattern yielded the highest tensile and flexural strengths at all infill percentages due to the alignment of deposited rasters with the loading direction. The Hilbert curve pattern also showed a significant increase in strength and modulus at 100% infill due to strong bonding between rasters resulting from shorter nozzle travel distances. SEM analysis revealed that concentric and Hilbert curve patterns had fewer and smaller voids, indicating stronger bonding between rasters compared to rectilinear and honeycomb patterns.

Gao et al., [18] provide a comprehensive study on optimizing fused deposition modelling (FDM) parameters to enhance the mechanical properties and surface quality of 3D-printed poly-ether-ether-ketone (PEEK). Their findings revealed that controlling crystallinity and minimizing porosity significantly improve tensile strength and surface finish. The research underscores the importance of adjusting nozzle temperature, printing speed, and annealing temperature to achieve properties comparable to injection-moulded parts, enhancing PEEK's potential for high-performance applications.

Ding et al., [19] investigated the effects of nozzle temperature and building orientation on the mechanical properties and microstructure of 3D-printed PEEK and PEI parts. The study found that the properties of printed parts were influenced by air pores formed during printing.

The mechanical properties of PEEK and PEI parts could reach about 80% of injection moulded parts after optimization. PEEK exhibited better toughness than PEI due to its semi-crystalline nature, while PEI was more brittle. The printing orientation also affected the mechanical properties, with horizontal printing generally resulting in better flexural and impact strength for PEEK.

The following literature specifically focuses on the study of tensile properties of PLA material in the context of additive manufacturing:

Corapi et al., [20] characterized the mechanical properties of polylactic acid (PLA) produced by fused deposition modelling (FDM) technology. The authors manufactured tensile test specimens in three different orientations (horizontal, on side, and vertical). The results showed that the specimens printed in the horizontal orientation exhibited the highest ultimate tensile strength and elastic modulus. The study also found that the fracture point location was more consistent in vertical specimens compared to the other two orientations.

Wang et al., [21] examined how FDM process parameters influence the tensile and dynamic mechanical properties of 3D printed PLA materials. Through uniaxial tensile tests and dynamic mechanical analysis, the effects of printing angle, layer thickness, fill rate, and nozzle temperature were characterized. The study highlighted the importance of optimizing these parameters to enhance the mechanical properties of FDM-printed materials, particularly under varying temperature conditions. They found that increased printing angle and fill rate improved tensile strength, while higher nozzle temperatures enhanced storage modulus.

Ambrus et al., [22] investigated the influence of printing parameters (orientation, fill pattern, and infill density) on the tensile properties of 3D printed copper-polylactic acid (PLA) composites. Horizontally printed samples were stronger than vertically printed ones due to different fracture mechanisms. Linear fill patterns resulted in higher tensile stress than cubic patterns. Increasing infill density generally improved strength, with 100% infill showing the

best results for linear fill and 50% infill for cubic fill. The optimal parameters for mechanical strength were horizontal printing, 100% infill, and linear fill pattern.

Imran et al., [23] studied the effect of FDM printing parameters (nozzle speed, infill rate, and layer height) on the mechanical properties (tensile, flexural, compressive strength, and shore hardness) of carbon particle-filled polylactic acid (PLA) composites. The study found that infill rate was the most significant parameter affecting the mechanical properties. The highest tensile strength was achieved with a moderate infill rate (75 mm) and moderate printing speed (80 mm/min). The flexural and compressive strengths were highest at the highest infill rate, while the layer thickness was the most critical parameter for shore hardness.

Atakok et al., [24] investigated the effects of fused deposition modelling (FDM) parameters on the tensile, three-point bending, and impact strength of 3D printed parts using PLA and recycled PLA (Re-PLA) filaments. The study used the Taguchi method to optimize the parameters, including layer thickness, infill density, and filament type. The results showed that layer thickness was the most significant factor affecting all three mechanical properties. The optimal parameters for the best tensile strength were found to be a layer thickness of 0.25 mm, an infill density of 70%, and PLA filament. The study also highlighted the potential of using recycled PLA filament for 3D printing, promoting environmental awareness.

Liu et al., [25] investigated the mechanical characteristics (tensile and flexural properties) of 3D-printed polylactic acid (PLA) composites with various additives (wood, ceramic, copper, aluminium, and carbon fibre) using fused deposition modelling (FDM). The study found that ceramic, copper, and aluminium-based PLA composites exhibited similar or improved mechanical properties compared to virgin PLA. The mechanical properties were influenced by build orientation and raster angle, with on-edge orientation and +45/-45 raster angles generally resulting in the highest strength and modulus. Wood and carbon fibre-based

PLA composites showed reduced mechanical properties due to defects like porosity and poor interlayer adhesion.

Vălean et al., [26] experimentally investigated the influence of printing orientation (0°, 45°, 90°) and size effect (different thicknesses) on the tensile properties of 3D printed polylactic acid (PLA) specimens using fused deposition modelling (FDM). The study found that printing orientation had a minor effect on Young's modulus but a more significant effect on tensile strength, with 0° orientation resulting in the highest tensile strength. Increasing the specimen thickness led to a decrease in both Young's modulus and tensile strength. The authors also analysed the dimensional accuracy of the printed specimens and found that the relative errors for thickness and width were below 4%.

Abeykoon et al. [27] Examined how infill density, infill speed, infill pattern, and the choice of materials impact the mechanical, thermal, and morphological properties of 3D-printed structures. The research revealed that a 100% infill density combined with a 90 mm/s infill speed resulted in the highest Young's modulus, with pure PLA reaching 1538.05 MPa. Among the five materials tested, carbon fibre reinforced PLA (CFR-PLA) exhibited the highest Young's modulus at 2637.29 MPa. The study also noted that voids and gaps between layers could initiate cracks and that the degree of PLA crystallinity did not significantly affect its mechanical properties

Rao et al., [28] investigated the effect of fused deposition modelling (FDM) parameters (layer thickness, extrusion temperature, and infill pattern) on the tensile strength of carbon fibre PLA. A full factorial design of experiments was conducted, and the results were analysed using ANOVA and regression analysis. The study found that the interaction between layer thickness-infill pattern and infill pattern-extrusion temperature significantly affected tensile strength. The highest tensile strength was achieved with a layer thickness of 0.1 mm, an extrusion

temperature of 225^0 C, and a cubic infill pattern. A regression model was developed to predict tensile strength based on the printing parameters.

Xu et al., [29] investigated the impact of thickness, scale, and printing sequence on the tensile and fracture properties of polylactic acid (PLA) specimens produced using fused deposition modelling (FDM). The study found that increasing build thickness improved elongation at failure and slightly increased ultimate tensile strength. Downscaling the specimens initially caused minor decreases in mechanical properties, but further reductions led to significant drops due to the increased ratio of intrinsic defects to specimen size. Fracture analysis revealed that larger build thickness and smaller scale resulted in lower fracture resistance. The printing sequence had a limited effect on mechanical performance. A boundary effect model was employed to evaluate fracture behaviour, demonstrating its applicability for fracture prediction of FDM parts with different scales and thicknesses.

Ma et al., [30] investigated the effect of printing angle on the mechanical properties of 3D-printed polylactic acid (PLA) specimens under uniaxial tensile and shear-tensile loading conditions. The authors found that the ultimate strength and strain of tensile specimens were highest when the printing angle was 0°/90°. The shear-tensile specimens showed different stress-strain behaviours and fracture morphologies depending on the slot angle and printing angle, with the strain distribution in the slot area becoming more uneven as the slot angle increased.

Pazhamannil et al., [31] used an artificial neural network (ANN) to predict the tensile strength of polylactic acid (PLA) parts produced using fused deposition modelling (FDM). The study considered three process parameters: nozzle temperature, layer thickness, and infill speed. Experimental data was collected using a Taguchi L9 orthogonal array, and the ANN was trained using this data. The results showed that layer thickness was the most significant factor affecting tensile strength, followed by nozzle temperature and infill speed. The developed ANN

model accurately predicted the tensile strength of PLA parts, with a correlation coefficient of 0.99982.

1.2.2 Literature survey on fatigue-fracture property of additively manufactured materials:

Yadollahi et al., [32] reviewed the current state of knowledge on the mechanical characteristics of metallic parts fabricated via additive manufacturing (AM), focusing on fatigue resistance. The authors discussed the challenges in achieving consistent mechanical properties due to microstructural heterogeneities and defects in AM parts. They emphasized the need to understand the relationships between process parameters, thermal history, microstructure, and mechanical behaviour to improve the reliability of AM parts. The review also highlighted the potential of microstructure-sensitive mechanical models and design optimization strategies to enhance the fatigue performance of AM materials.

Shanmugam et al., [33] analysed the fatigue behaviour of 3D-printed polymers, architected cellular materials (ACMs), polymeric composites, produced using fused deposition modelling (FDM). The authors explored how FDM printing parameters—including infill density, build orientation, layer height, nozzle diameter, raster angle, and printing speed—along with material properties, affect fatigue life. The review also emphasized the importance of fatigue assessment for biomedical materials produced by FDM and discussed the challenges in comprehending the fatigue behaviour of novel FDM-printed ACMs due to their intricate geometries and potential stress concentrations.

Sharafi et al., [34] reviewed the factors that influence the fracture toughness of extrusion-based additively manufactured polymer and polymer composites. The authors identified three main categories of factors: deposition, solidification, and composition/rheology. They discussed best practices to improve fracture toughness and address fracture behaviour in 3D printed parts, focusing on the fused filament fabrication (FFF)

method. The review also identifies gaps in the literature and discusses the future outlook of AM using FFF.

Gardan et al., [35] examined methods to improve fracture toughness in 3D-printed materials using extrusion deposition. By employing finite element simulation to align filament deposition with principal stress directions, they observed enhanced mechanical characteristics in ABS samples. Crack branching was analysed, revealing that optimized filament paths significantly improved fracture toughness compared to classical methods. Their results suggested a strategic reinforcement of printed structures by adapting deposition trajectories to mechanical stresses.

He et al., [36] studied effects of 3D printing parameters on crack growth in ABS parts under heat and stress. They used ABS beams with different build angles, nozzle sizes, and layer thicknesses at high temperatures. Results suggested a 0° angle, 0.8mm nozzle, and 0.15mm layer thickness performs best. Further tests with a 0.4mm nozzle at 50°C revealed the X orientation has the slowest crack growth, while the Y orientation cracks fastest.

Azadi et al., [37] investigated the impact of print direction on the fatigue properties of FDM printed parts made of PLA and ABS, samples printed in horizontal and vertical directions with a 0.15 mm layer thickness and 50% infill. Rotary bending fatigue tests were conducted under fully-reversed stress-controlled loading at various stress levels and the results showed that horizontally printed specimens had higher fatigue strength compared to vertically printed ones with PLA outperforming ABS in fatigue lifetime. SEM analysis revealed beach marks on PLA fracture surfaces, indicating cyclic loading. The fatigue strength exponent and coefficient were calculated, with horizontal samples exhibiting better fatigue properties overall.

Khan et al., [38] reviewed recent advancements in enhancing the fracture toughness of 3D-printed fibre-reinforced polymer composites (FRPCs). The authors emphasized that the layer-by-layer nature of additive manufacturing makes these composites susceptible to

delamination. The review discusses strategies to improve fracture toughness, including optimizing printing parameters like temperature, speed, and layer thickness, as well as post-processing techniques like surface treatment and annealing. The authors also highlighted the properties of common 3D printing materials, such as PLA and PEEK, and their use in various applications. The review concludes by identifying current challenges and future directions in the field.

Rezaeian et al., [39] Explored how printing speed influences the and fracture and tensile behaviour of ABS samples made through fused deposition modelling (FDM). The study revealed that specimens printed at 70 mm/s showed the greatest elongation, ductility, and fracture resistance compared to those printed at slower speeds ($10, 30, and\ 50\ mm/s$). This enhanced performance at 70 mm/s was linked to improved bonding between the deposited lines and layers, leading to fewer air gaps and reduced filament pullout. Additionally, the authors also indicated that the fracture growth path in semicircular bending (SCB) specimens was largely unaffected by printing speed.

Qu et al., [40] examined how the presence of double cracks impacts the fatigue crack growth life (FCGL) of a additively printed compressor impeller made from Ti-6Al-4V alloy, fabricated using selective laser melting (SLM) Their study involved numerical simulations of the printing process, heat treatment, and actual working conditions to determine crack initiation locations and stress intensity factors. The results showed that the middle and root of the blade were prone to crack initiation. The FCGL was analysed for single and double crack scenarios under different rotational speeds, revealing that the presence of double cracks significantly reduced the FCGL compared to single cracks, especially at high speeds. The study highlights the importance of considering residual stress from 3D printing and the impact of multiple cracks in damage tolerance assessments of compressor blades.

Ramadas et al., [41] analysed the fracture toughness and fatigue crack growth (FCG) rate of Precipitation Hardening Stainless Steel (PH SS) produced by Laser Powder Bed Fusion (L-PBF). The study evaluates the effect of notch orientation whether parallel or perpendicular to the build direction on fracture toughness and FCG, comparing L-PBF samples in solution annealed (SA) and SA + aged conditions to those of wrought PH SS. Findings show minimal impact of orientation on FCG up to a stress intensity factor range (ΔK) of 30 MPa√m, with higher rates observed beyond this point. L-PBF specimens exhibited lower fracture toughness compared to wrought material, attributed to defects inherent in the additive manufacturing process. Specimens with horizontal notches demonstrated higher fracture toughness (51–62 MPa√m) than those with vertical notches (40–46 MPa√m).

Khosravani et al., [42] explored the fracture behaviour of single lap joints (SLJs) which are bonded using adhesives and fabricated from 3D-printed PETG using fused deposition modelling (FDM). The research focused on how raster angle, raster width, layer thickness, and adhesive layer thickness influence the mechanical property and failure mechanism of these joints. Findings indicated that thinner adhesive layers (0.2 mm) resulted in higher fracture loads, with cohesive failure being the predominant failure mode. Additionally, a finite element model was created to simulate stress distribution and the progression of failure within the adhesive layer, offering insights into the fracture behaviour of 3D-printed PETG joints.

Leuders et al., [43] investigated the crack growth and fatigue resistance performance of TiAl6V4 alloy fabricated using selective laser melting (SLM). The study found that post-processing treatments such as hot isostatic pressing (HIP) and heat treatment significantly improved the material's fatigue properties. Heat treatment reduced residual stresses, leading to better crack growth resistance, while HIP minimized porosity, enhancing fatigue strength to match conventionally processed Ti-6-4. The authors concluded that optimizing SLM process

parameters and post-processing techniques can mitigate the negative effects of process-induced imperfections and improve the mechanical behaviour of SLM-produced TiAl6V4.

Azadi et al., [44] investigated the influence of direction during printing (horizontal and vertical) on the high-cycle bending fatigue properties of 3D-printed PLA and ABS polymers using FDM. The results indicated that ABS specimens exhibited poorer fatigue lifetimes compared to PLA specimens. Horizontally printed samples exhibited higher fatigue strength than vertically printed samples for both materials. The stress level, material type, and print direction were statistically significant factors influencing fatigue life. SEM analysis revealed beach marks on the fracture surface of PLA specimens, indicating cyclic loading and brittle fracture

Smudde et al., [45] investigated the influence of residual stress on the fatigue crack growth of additively manufactured (AM) Type 304L stainless steel produced by directed energy deposition (DED) compared to wrought Type 304/304L. The study found that tensile residual stresses in DED material led to faster crack growth rates than wrought material at the same applied stress intensity factor range. However, after correcting for residual stress and crack closure effects, the intrinsic fatigue crack growth rates of both materials were similar at lower stress intensity factors, with DED material showing slightly lower rates at higher values. The study highlights the importance of considering residual stress in assessing the fatigue performance of AM materials.

Daynes et al., [46] investigated the fracture toughness of additively manufactured Ti-6Al-4V lattice structures using extended compact tension (EC(T)) specimens. The study found that fracture toughness increased with relative density and crack length. A finite element analysis (FEA) model validated the experimental results and revealed that stress redistribution near the crack tip caused the increase in toughness with crack growth. The authors also

proposed a size optimization methodology to enhance the initial fracture toughness of lattice structures, demonstrating up to a 37% increase in toughness.

Paul et al., [47] emphasized the importance of evaluating fracture toughness independently from ductility when developing additively manufactured (AM) metals for structural applications. The authors argued that while ductility is often used as a proxy for fracture toughness, the correlation between the two properties is weak, especially in AM materials due to their unique microstructures and processing-related defects. The authors analysed data for Al-, Fe-, and Ti-based alloys produced by both conventional and AM methods, highlighting cases where materials with similar ductility exhibited vastly different fracture toughness values. They concluded that an independent assessment of fracture toughness is crucial for optimizing AM processes and ensuring the reliability of AM parts in structural and safety-critical applications.

The following literature specifically focuses on the study of fatigue and fracture behaviour of PLA material in the context of additive manufacturing:

Dadashi et al., [48] examined how print parameters including print temperature, print speed, and nozzle diameter affect the fatigue life of PLA through rotating bending fatigue tests. The authors created a regression model to estimate fatigue life based on these parameters and discovered that the optimal fatigue life was achieved with a print speed of 5 mm/s, a print temperature of 210°C, and a nozzle diameter of 0.2 mm. Scanning electron microscopy analysis of the fracture surfaces showed evidence of crazing, even though PLA exhibited brittle behaviour.

Senatov et al., [49] studied low-cycle fatigue behaviour of additively printed PLA and mix of PLA and 15% wt. Hydroxyapatite powder porous scaffolds for bone replacements. The study found that the scaffolds underwent a decrease in height, pore collapse, delamination, and crack growth under cyclic loading. The incorporation of HA particles enhanced crack

resistance and decreased the rate of defect accumulation compared to scaffolds made of pure PLA. The PLA/HA scaffolds showed potential for use as bone implants, capable of functioning under cyclic loading at a stress of 21 MPa for extended periods without significant changes.

Vălean et al., [50] investigated the impact of crack insertion on Mode I and Mode II fracture toughness in FDM printed PLA materials. Using Single Edge Notch Bend specimens, the study compared notches made by 3D printing and milling. The results indicated that specimens with 3D printed notches had higher fracture toughness than those with milled notches. The effect was more pronounced in Mode I fracture toughness and less significant in Mode II.

Milovanović et al., [51] investigate crack path direction in plane-strain fracture toughness tests of quasi-brittle PLA and ductile PLA-X composite using FDM techniques. The study reveals that PLA typically exhibits a brittle fracture pattern with straight crack paths, while PLA-X demonstrates ductile behaviour with more tortuous crack paths. The results emphasize that layer height, infill density, and printing orientation significantly influence fracture behaviour, suggesting that PLA-X offers enhanced toughness and resistance to crack propagation compared to PLA**.**

Papon et al., [52] studied the fracture properties of 3D printed polylactic acid (PLA) and short carbon fibre (CF) reinforced PLA composites. The authors used fused filament fabrication (FFF) with both circular and square nozzles and investigated the effects of CF reinforcement, nozzle geometry, and bead lay-up orientation. The results showed that adding CF improved fracture toughness and energy, with 5 wt% CF showing the most significant improvement. Square nozzles enhanced fracture toughness due to reduced inter-bead voids and larger bonded areas compared to circular nozzles. The study also examined crack propagation and fracture mechanisms using microscopy.

Bakhtiari et al., [53] investigated the impact of 3D printing parameters on the quasi-static and fatigue properties of polylactic acid (PLA) bone scaffolds. The study found that extrusion width was the most significant factor affecting quasi-static compressive properties, while nozzle temperature was the most significant factor influencing fatigue performance. Scaffolds printed at a lower nozzle temperature exhibited higher fatigue resistance. The study also found that all scaffolds were safe for bone applications under the studied conditions, as the maximum strain amplitude induced on natural bone in daily activities is lower than the strain amplitudes tested in the study.

Kizhakkinan et al., [54] experimentally investigated the fracture toughness of 3D printed polylactic acid (PLA) parts fabricated using fused deposition modelling (FDM). The study examined the effects of printing speed (20-60 mm/s) and filament orientation (0/90 and 45/45 degrees) on fracture toughness using compact tension (CT) specimens. The results showed that fracture toughness decreased at higher printing speeds, while the energy absorbed before failure increased. The 45/45 filament orientation exhibited higher fracture toughness compared to the 0/90 orientation. Tensile tests on PLA filaments and printed coupons revealed that filaments had higher stiffness and strength due to the absence of voids formed during printing.

Khosravani et al., [55] investigated the effects of printing parameters (raster orientation and printing speed) on the fracture toughness of 3D-printed polylactic acid (PLA) parts using compact tension (CT) tests. The results showed that the fracture load decreased with increasing printing speed, likely due to reduced bonding between filaments at higher speeds. The highest fracture load was observed in specimens printed at 20 mm/s with a 45/-45 raster orientation, while the lowest fracture load was found in specimens printed at 80 mm/s with a 0/90 raster orientation. The crack growth direction was also influenced by the raster

orientation, propagating parallel to the initial crack in 0/90 specimens and at a 45-degree angle in 45/-45 specimens.

Shahar et al., [56] investigated the density, fatigue, and impact strength of 3D printed kenaf/PLA composites for potential use in ankle-foot orthoses (AFOs). The study found that increasing kenaf filler content decreased density and impact resistance but improved fatigue life. The authors concluded that kenaf/PLA composites show promise for AFO applications due to their lightweight nature and fatigue properties, but further research is needed to improve impact resistance.

1.3 Summary of literature survey:

Tensile Properties

- **Influence of printing parameters:** Various studies have investigated the impact of printing parameters such as layer thickness, infill density, printing orientation, raster angle, nozzle temperature, and printing speed on the tensile properties of different materials (PLA, ABS, PETG, composites). These parameters significantly influence the strength, stiffness, and ductility of the printed parts.
- **Material properties:** The choice of material also plays a crucial role in determining the tensile properties. For example, PETG generally exhibits higher tensile strength and elongation compared to PLA and ABS.
- **Comparison with traditional manufacturing:** Some studies have compared the tensile properties of 3D printed parts with those produced by injection moulding. While injection-moulded parts may have higher yield strength, 3D printed parts can achieve comparable or even superior properties in terms of ultimate tensile strength and ductility with proper parameter optimization.
- **Composite materials:** The addition of fillers like carbon fibre, wood, ceramic, copper, and aluminium to PLA can modify its mechanical properties. Some fillers improve

tensile strength and stiffness, while others may reduce them due to defects like porosity and poor interlayer adhesion.

Fracture and Fatigue Properties

- **Fracture toughness:** Studies have investigated the fracture toughness of 3D printed polymers and composites, examining the effects of printing parameters, notch insertion methods, and material composition. The results show that optimizing printing parameters and using appropriate materials can improve fracture toughness.
- **Fatigue behaviour:** Research has also focused on the fatigue performance of 3D printed polymers, composites, and metals. The studies have explored the influence of printing parameters, material properties, and post-processing techniques on fatigue life and crack growth resistance.
- **Challenges and future directions:** The literature review highlights the need for further research to understand the complex relationships between process parameters, microstructure, and mechanical behaviour in 3D printed parts. This knowledge is crucial for developing reliable and durable components for various applications, including biomedical, aerospace, and automotive industries.

Overall, this literature review offers a thorough summary of existing research on the mechanical properties of additively printed components, emphasizing significant discoveries, ongoing challenges, and potential future developments in this rapidly advancing field.

1.4 Research Gap:

While additive manufacturing has gained significant attention in recent times, particularly with the application of PLA (Polylactic Acid) as a filament material, there remains a notable gap in understanding the effect of different infill densities and patterns on the mechanical properties of additively printed specimens. Most of the existing literature has focused on the general mechanical performance of PLA under varying conditions, but there is

limited research specifically addressing the comparative effects of different infill densities, particularly at 25%, 50%, and 100%, combined with the honeycomb infill pattern which is well-known for its high strength to weight ratio and energy absorption capabilities, is specifically chosen to explore its potential in enhancing the mechanical properties of additively printed PLA.

Moreover, while tensile testing has been widely explored, there is a lack of comprehensive studies that also integrate Fatigue Crack Growth Rate (FCGR) and fracture testing within the same set of experiments. These mechanical tests are crucial for determining the durability and failure characteristics of 3D-printed components, especially those that are subjected to cyclic loads and potential crack propagation in practical applications.

This study seeks to address this gap by methodically examining the tensile strength, fatigue crack growth rate and fracture toughness of PLA specimens with different infill densities and a honeycomb infill pattern. This approach aims to offer a comprehensive understanding of PLA's mechanical performance under various conditions, thereby providing valuable insights into the field of additive manufacturing.

1.5 Objective of this Thesis:

1. To fabricate FDM printed PLA specimen adhering to the ASTM standards (ASTM D638 for tensile specimen, ASTM E647-15 for FCGR specimen and ASTM E1820-13 for fracture toughness specimen). For that corresponding CAD file have to be drawn.
2. To study the effect of infill density on tensile properties (Yield stress, Ultimate stress, Young's modulus and percentage elongation), for that tensile tests are carried out in room temperature with $0.001s^{-1}$ strain rate according to the ASTM D638 standard. Comparison study of the tensile properties of different infill density material is also conducted from the test results.

3. To find the Paris exponent, Paris constant and Threshold stress intensity factor by carrying out FCGR test according to the ASTM E647-15 standard. From the generated a vs N data using secant method $\frac{da}{dN}$ vs ΔK plot is to be plotted.
4. To study the effect of infill density on fracture toughness (J_{1C}) and crack initiation fracture toughness (K_{JC}), for that fracture toughness tests are carried out according to the ASTM E1820-13 standard and crack initiation fracture toughness is computed from the empirical equation with the help of J_{1C} .

Chapter 2: Additive Manufacturing

2.1 Introduction:

Additive manufacturing, commonly referred as 3D printing worldwide, has the potential to usher in a similar societal revolution, affecting every facet of our lives. An extensive amount of research has been devoted to its technical aspects, covering materials, processes, applications, and management. This chapter provides brief overview of these technologies, starting with an introduction to additive manufacturing, followed by discussions on their current applications and future potential areas of use.

2.2 Definition and History of Additive Manufacturing:

Additive manufacturing (AM) refers to a technology that fabricates physical objects from digital three-dimensional (3D) models by assembling them layer by layer until the final product is complete. This approach differs from subtractive manufacturing, where a solid block of material is shaped by removing excess material to achieve the desired form. In contrast, additive manufacturing constructs the object by sequentially adding each layer on top of the previous one. The thickness of these layers can vary from a few microns to about 0.25 mm, depending on the specific technique employed. A wide range of materials can be utilized in different AM processes.

The initial ideas behind additive manufacturing can be traced back to the end of the 19th century and the start of the 20th century. This era introduced the use of topographical maps as three-dimensional representations of terrain, and methods were developed to create 3D maps by superimposing paper maps onto these topographical models. Additionally, photo sculpture, which emerged in the late 19th century and bore some resemblance to the early stages of CNC machining, proposed techniques for forming models using photosensitive substances.

The origins of contemporary additive manufacturing date back to the mid-20th century, notably with Otto John Munz's 1951 patent [57], which set the stage for stereolithography. Munz's

technique involved layer-by-layer exposure of a transparent photo emulsion to construct a cross-sectional representation of an object. However, a limitation of this method was that the resulting 3D structure required manual carving or etching from the cylinder.

In the following decades, numerous new techniques were developed, including Swainson's 1968 suggestion for creating plastic patterns by selectively polymerizing 3D structures with

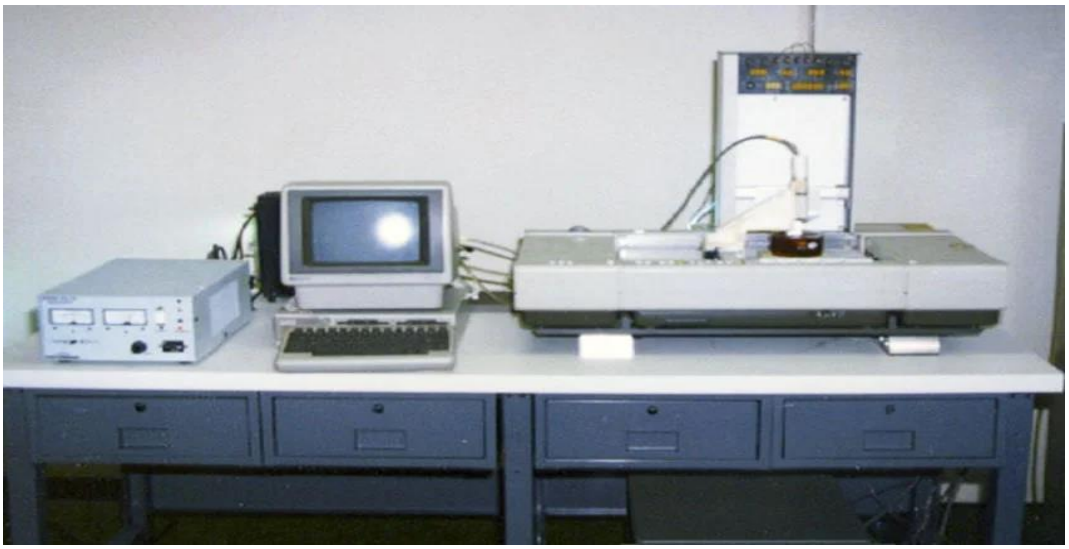

Fig 2.1: Stereolithography apparatus developed by Charles Hull in 1986

intersecting laser beams. [58]. Ciraud's 1971 powder process [59] and Housholder's 1979 powder laser sintering process [60] further advanced direct deposition AM methods. These developments laid the foundation for the commercialization of additive manufacturing systems, notably Charles W. Hull's 1986 stereolithography (SLA) patent, which is depicted in Fig 2.1 led to the establishment of 3D Systems in 1988 and the first commercial SLA machine [61].

The terminology used to describe additive manufacturing has changed over the years. In the 1990s, it was commonly known as rapid prototyping. Efforts to standardize the terminology led to the ASTM International Committee F42 formally adopting "Additive Manufacturing" in 2009 [62]. Unlike subtractive manufacturing, which shapes the final product

by removing material, additive manufacturing builds up the product layer by layer, minimizing waste and reducing production time and costs. Although the industry has largely accepted the term "Additive Manufacturing," the term "3D printing" remains prevalent in popular media due to its widespread recognition among the general public.

2.3 Current Usage of Additive Manufacturing

Over the past thirty years, additive manufacturing (AM) has grown substantially across various application areas. The Wohlers Report[63], a key annual industry assessment, regularly surveys the extent of AM adoption . The 2011 edition highlights several application areas for AM, as depicted in Fig 2.2.

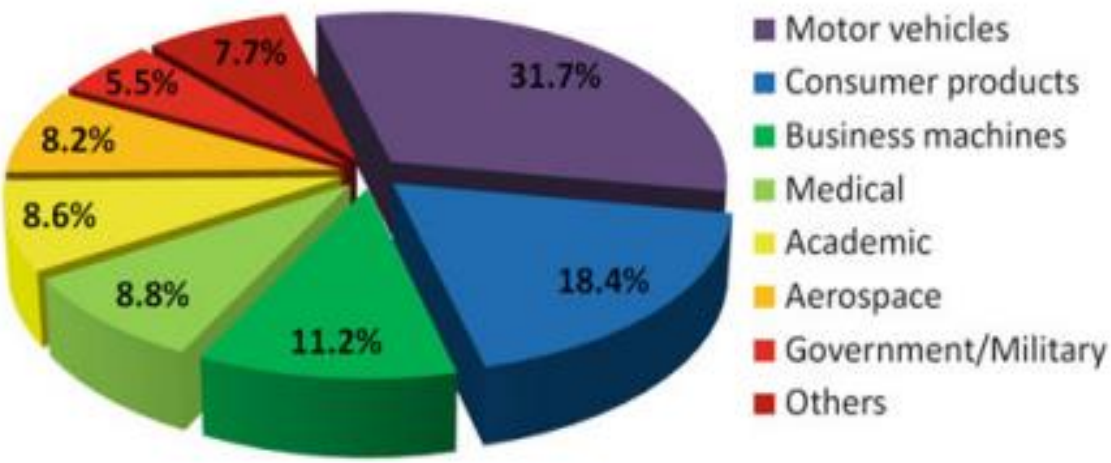

Fig 2.2: Application of 3D printing [64]

Notably, over 52% of AM applications pertain to rapid prototyping activities, such as assembly testing, functional and demonstration models, and visual aids. Meanwhile, the use of AM for producing concrete parts, both directly and indirectly, accounts for nearly 39% of total usage. This includes creating prototype tools, metal casting models, tool components, and directly manufacturing parts. Wohlers anticipates significant growth in this percentage in the coming years.

Additive manufacturing has evolved along two distinct paths. Over the last decade, there have been notable advancements in state-of-the-art machines that produce high-quality parts from a variety of materials. Concurrently, the DIY 3D printing community has flourished, characterized by affordable entry-level plug-and-play systems priced from a few hundred to a few thousand dollars. Communities such as **Reprap, Fablab**, and **Makerbot**, which often embrace an open-source philosophy, have emerged, disseminating additive manufacturing knowledge and enriching the field.

Furthermore, the increasing adoption of AM across industries highlights its rising significance. Only in recent years has AM achieved a level of quality that allows some companies to consider it a viable manufacturing technology. As polymer and metal materials continue to advance and machines become faster and more precise, additive manufacturing is likely to be increasingly integrated into conventional production lines such as Rapid Prototyping and Iteration, Hybrid Manufacturing, Tooling and Fixture Production. Additionally, AM possesses unique capabilities that enable the production of parts unachievable through traditional manufacturing techniques.

2.4 Additive Manufacturing Process

Additive manufacturing (AM) converts a digital CAD model into a physical object through a series of precise steps. The degree to which AM is integrated into the production process can vary widely based on the product's complexity and size. In the initial phases of product development, AM is often used to quickly produce rough prototypes due to its rapid turnaround. As development advances, these parts may undergo thorough cleaning and post-processing, which can include sanding, surface finishing, and painting. AM is particularly beneficial in this stage as it enables the creation of intricate designs without the limitations of traditional manufacturing methods. Typically, most AM processes involve the following six steps to some extent as seen in Fig 2.3.

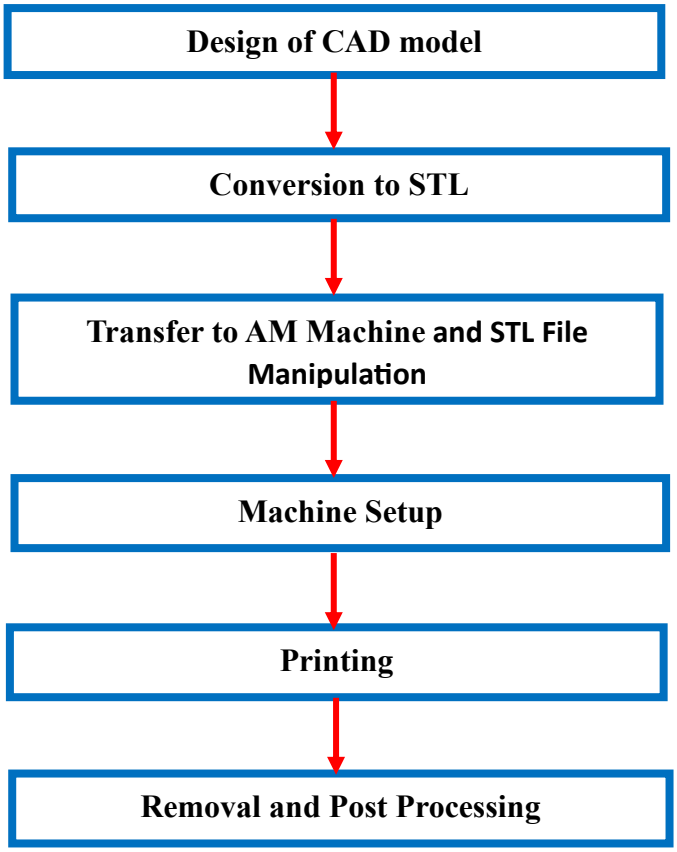

Fig 2.3: Steps Involved in Additive Manufacturing Process

Design of CAD model: Each additive manufacturing component starts with a digital model that fully defines its external shape. This involves using various advanced Computer-Aided Design (CAD) software to produce a 3D solid or surface model. Alternatively, reverse engineering techniques, such as laser and optical scanning, can be used to generate this 3D representation. Figure 2.4 illustrates the CAD modelling of a Compact Tension specimen.

Conversion to STL File: STL files are simple depiction of a 3D object's surface. The object is broken down into countless tiny triangles as shown in Fig 2.5, defining each triangle by its outward-facing direction (normal) and the coordinates of its three corners (vertices). This triangular mesh is then used by 3D printers to construct the object layer by layer.STL encodes a surface geometry using a concept called **TESSELATION**, it is a process of filling a surface with one or more geometric shapes such that there is no overlap or gaps.

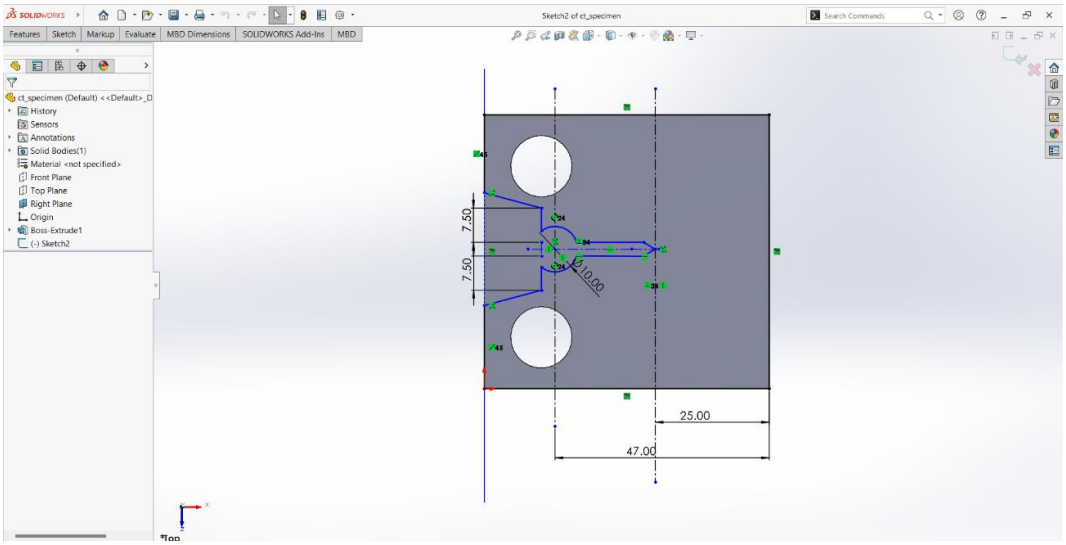

Fig 2.4: CAD Modelling in CAD software

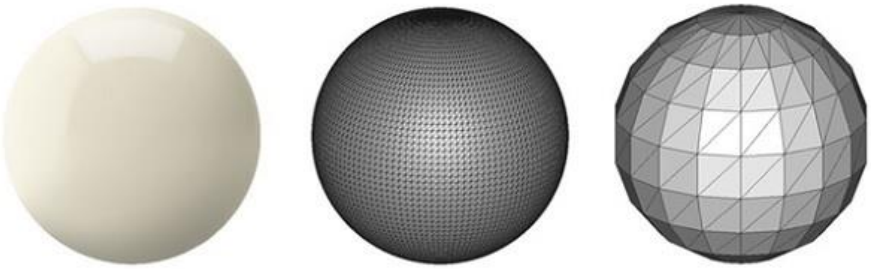

Fig 2.5: STL file conversion for 3d Printing

STL file pre-processing and transfer for AM build preparation: After that the STL file is transferred to a slicing software and input parameters like infill density, infill structures, supports etc. used to obtain the G-Code, which is then fed to the AM machine.

Machine Configuration: Prior to beginning of printing, the AM machine needs to be correctly configured. This setup includes configuring parameters related to the printing, such as the power source, layer height, timing, and material constraints.

Printing: The majority of the printing process is automated, and the machine may function largely unattended. The machine can now operate with minimal oversight, with checks in place to identify any issues like material depletion, power failures, or software glitches.

Removal and Post Processing: After the printing process is finished, the parts need to be removed from the additive manufacturing machine. This step may involve interacting with the

machine, including engaging safety interlocks to ensure that there are no moving parts or that operating temperatures remain within safe limits. At this stage, the parts may be fragile or have support structures that must be removed. Consequently, this often requires careful, skilled manual work and can be time-consuming

2.5 Classification of AM as per ASTM:

ISO/ASTM 52900 in 2015 [65], delineated seven classifications for additive manufacturing as depicted in Fig 2.6. These encompass material extrusion, material jetting, directed energy deposition, powder bed fusion, binder jetting, vat polymerization, and sheet lamination. It's notable that researchers are actively developing all of these mentioned categories to enhance the efficiency of manufactured components.

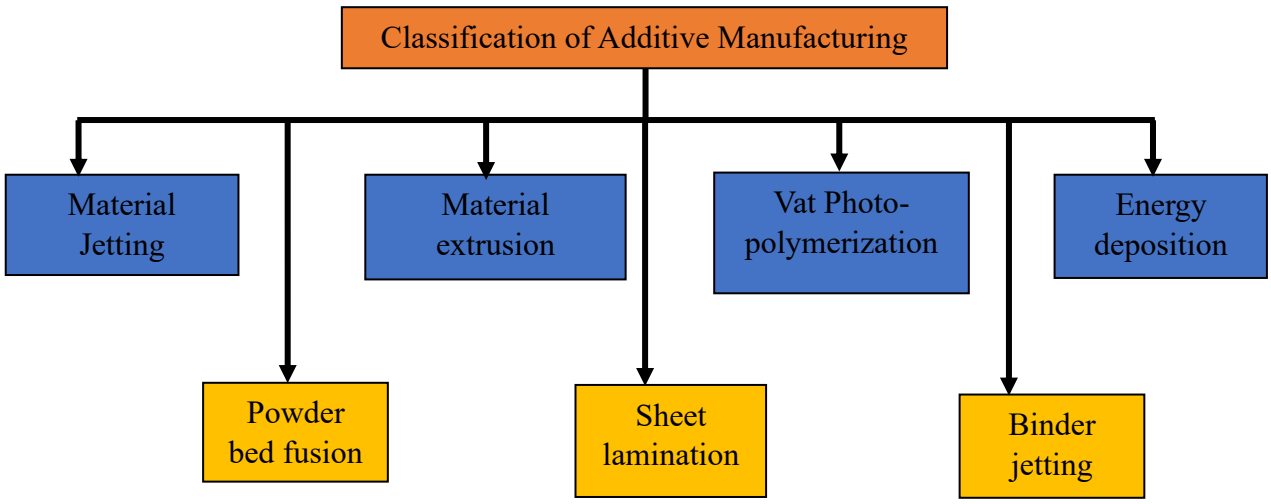

Fig 2.6: Classification of Additive Manufacturing according to ASTM 52-15

The previous section offered a comprehensive overview of additive manufacturing (AM) process classification, categorized according to the methodology for product formation as per ISO/ASTM 52900 in 2015, the type of base material utilized, and the medium employed for processing.

The subsequent focus on Material Extrusion is motivated by the specific context of this thesis. The specimens used in the experimental investigations were fabricated using an extrusion-

based 3D printer, specifically employing Fused Deposition Modelling (FDM). Therefore, a deeper dive into Material Extrusion techniques, with a particular emphasis on FDM, is warranted to provide the necessary background and understanding for the subsequent chapters that detail the experimental procedures and results.

The deliberate transition from a general classification of AM to a focused exploration of Material Extrusion aligns with the practical constraints of the research, where access to 3D printers was limited to those based on extrusion technology. This limitation, while acknowledged, does not undermine the significance of the research, as it enables a thorough examination of the mechanical properties of 3D printed PLA material fabricated using FDM, contributing valuable insights to the field of additive manufacturing.

2.5.1 Material Extrusion

Material extrusion processes are similar to applying icing on a cake, where material stored in a container is pushed through a small diameter opening due to applied force. With steady pressure, the extruded material, commonly known as 'roads,' maintains a uniform flow rate and diameter. This diameter stays constant as the nozzle moves across a surface at a steady speed that matches the flow rate. The material exiting the nozzle must be semi-solid, solidifying completely while retaining its shape. Additionally, it must adhere to previously extruded material to form a solid structure. Given the extrusion of material, the additive manufacturing (AM) machine needs to scan horizontally and control material flow by starting and stopping it during scanning. After completing a layer, the machine must either move upward or lower the part to enable the creation of the next layer.

Two primary approaches are employed in extrusion processes. The predominant method involves temperature control to manipulate the material state. Here, material in a reservoir is melted to a liquid state for extrusion from the nozzle, bonding with earlier deposited material

before solidifying. A schematic illustration of Material extrusion process can be seen in Fig 2.7.

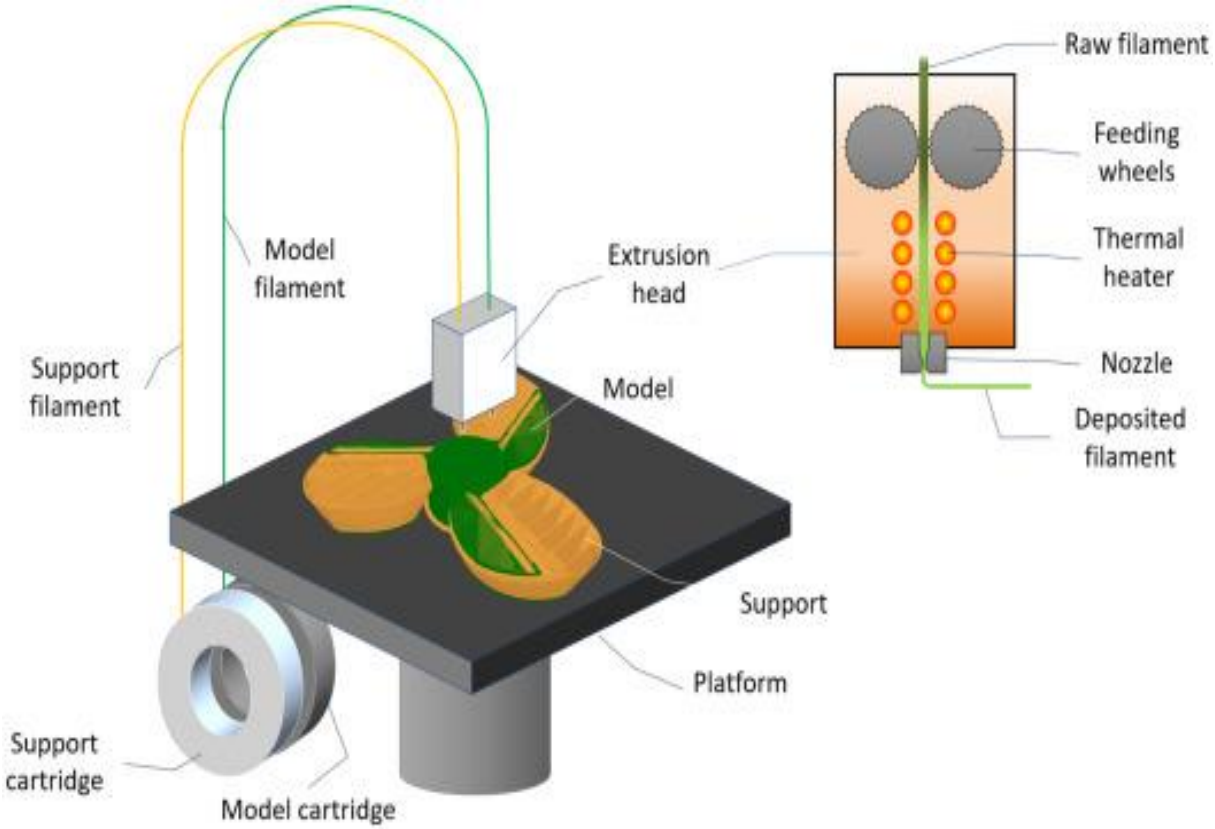

Fig 2.7: Material Extrusion Process

An alternative method relies on chemical changes to induce solidification. This may involve the introduction of a curing agent, evaporation of a solvent, reaction with air, or the drying of a "wet" material to facilitate bonding. Parts can undergo curing or drying to achieve stability, particularly when using paste materials. This approach is especially pertinent in biochemical applications where materials must exhibit biocompatibility with living cells, thus necessitating strict material selection. However, it may also find industrial applications, potentially leveraging processes akin to reaction injection moulding, instead of solely relying on thermal effects. Types of commonly used material extrusion-based additive manufacturing processes include Fused Deposition Modelling (FDM), Direct Ink Writing (DIW), Robocasting also known as ceramic or paste extrusion, Bioprinting, Composite Filament Fabrication (CFF).

The preceding section provided a comprehensive overview of Material Extrusion as a category within Additive Manufacturing processes. The subsequent focus on Fused Deposition Modelling (FDM) is motivated by the specific methodology employed in this research. The specimens utilized in the experimental investigations were fabricated using FDM, which is a widely recognized and accessible extrusion-based 3D printing technique.

The deliberate emphasis on FDM is not only due to its prevalence but also stems from the practical constraints of the research, where the available 3D printers were exclusively based on FDM technology. This limitation, while acknowledged, does not diminish the value of the research, as it allows for a focused and in-depth exploration of the mechanical testing parameters of 3D printed PLA material produced through FDM. The subsequent sections will delve into the fundamentals of FDM, its process parameters, and commonly used materials, providing the necessary context for understanding the experimental procedures and results presented in the following chapters.

2.5.2 Fused Deposition Modelling (FDM)

The typically used extrusion-based additive manufacturing (AM) process is fused deposition modelling (FDM), which was developed by Stratasys, USA. FDM utilizes a heated chamber to melt material provided as thin filaments. This filament is fed into the chamber through a tractor wheel mechanism that creates the extrusion pressure.

However, a major limitation of FDM is its build speed. Due to the inertia of the plotting heads, FDM systems generally operate at lower maximum speeds and accelerations compared to other AM technologies. Additionally, FDM involves depositing material in a point-by-point, vector-based manner, requiring frequent directional changes.

2.5.3 FDM Process Parameters:

The performance of FDM parts is influenced by several factors, including printing parameters, bonding characteristics, material composition, and the presence of process defects. These factors collectively complicate the analysis of mechanical strength.

To further develop FDM technology and maximize the efficiency of materials fabricated by FDM, it is crucial to carefully examine the complex ways in which these materials break down. Research has concentrated on understanding how FDM based polymers and composites fail, especially in terms of their ability to withstand impact, bending, tensile and compressive loads and changes in temperature and pressure when subjected to steady forces.

Printing parameters:

The primary print parameters utilized in FDM 3D printing encompasses:

Layer Thickness: This refers to the height of each layer made in 3D, measured along the vertical axis. If the layers are made thinner, more layers are needed to finish the object, which takes longer to make. In general, optimum FDM layer height is between 0.17 mm and 0.33 mm.

Printing Temperature: The temperature at which the thermoplastic filament is melted and extruded through the print nozzle. This temperature varies according to the filament type such as Acrylonitrile Butadiene Styrene (ABS), Polyethylene Terephthalate Glycol (PETG), Polylactic acid (PLA), crucial for ensuring proper material flow and interlayer adhesion.

Bed Temperature: Pertinent for printers with a heated build platform, bed temperature facilitates improved adhesion of the initial layer to the build surface. Recommended temperatures vary depending on the filament type, with some, like ABS, necessitating heated beds to mitigate warping.

Printing Speed: Dictates the speed of the print head or build platform movement during printing, measured in millimetres per second (mm/s). Higher speeds reduce print time but may

compromise surface quality and accuracy, with lower speeds preferred for intricate details.

Infill Density: Represents the percentage of internal infill material within the printed object, providing structural support and reducing material consumption. Higher infill percentages yield stronger objects, while lower percentages conserve material and shorten print time. Infill pattern is closely associated with infill density.

Infill pattern: defines the internal geometry or structure of the infill, such as grid, honeycomb, or triangular. The combination of infill pattern and density allows users to customize the properties of their 3D printed objects to meet specific requirements.

Wall Thickness: Determines the thickness of the outer shell of the printed object, impacting its strength and structural integrity. Typically set as a multiple of the layer height to ensure consistent printing.

Top and Bottom Layers: Control the number of solid layers printed at the top and bottom surfaces of the object, enhancing strength and concealing infill patterns.

Retraction Settings: Manage filament withdrawal during non-printing movements to minimize stringing and oozing, enhancing surface quality and reducing post-processing requirements.

Cooling Fan Speed: Regulates the cooling fan's speed to prevent overheating and warping, particularly for intricate details.

Raster Angle: Specifies the orientation of printed layers or infill pattern relative to the build platform's X-Y plane, determining material deposition direction. Common values include 0°, 45°, and 90°, set in degrees.

2.5.4 Types of materials commonly used in FDM:

The material undergoes melting within a heated print nozzle and is subsequently deposited layer wise to construct a 3D object. FDM 3D printing boasts a diverse array of

materials, each possessing distinct properties and applications. Below are several common types of materials utilized in FDM 3D printing:

- **PLA (Polylactic Acid):** A popular, easy-to-use material known for its biodegradability and wide range of colours. Ideal for beginners and general-purpose prints.
- **ABS (Acrylonitrile Butadiene Styrene):** Stronger and more impact-resistant than PLA, but prone to warping and requiring a heated bed. Suitable for functional prototypes and durable objects.
- **PETG (Polyethylene Terephthalate Glycol):** A hybrid of PLA and ABS, offering a good balance of strength, flexibility, and ease of printing. Often used for bottles and containers.
- **TPU (Thermoplastic Polyurethane):** A flexible, rubber-like material commonly used for phone cases, wearables, and other applications requiring elasticity.
- **Nylon:** A strong and durable material with excellent abrasion resistance. Used in engineering applications, gears, and functional parts.
- **Specialty Filaments:** These include conductive, glow-in-the-dark, and wood-filled filaments, offering unique properties for specific projects.

Choosing the right material depends on the desired properties, printing experience, and intended application of the printed object.

For preparing tensile and fracture-fatigue testing specimens PLA material is chosen due to its popularity, ease of use, and versatility as a general-purpose 3D printing material. These characteristics make it particularly suitable for research projects, especially when exploring the mechanical properties of additively manufactured parts. Additionally, PLA's biodegradability aligns with the increasing emphasis on sustainable materials in research and development.

Chapter 3: Tensile Testing of Additively Manufactured PLA Specimens

3.1 Introduction:

In this chapter tensile properties of PLA samples have been studied with varying infill densities of 25%, 50% and 100% each having Honeycomb infill pattern. These 3 types of PLA samples have been additively manufactured using Fused Deposition Modelling (FDM) process according to the ASTM D638[66] standard. Tensile tests have been carried out in servo electro hydraulic INSTRON universal testing machine using constant displacement rate. Based on these experimental studies, different mechanical properties i.e., Young's modulus, yield strength, ultimate tensile strength and percentage of elongation have been measured. Along with comparison studies have been carried out by compiling the obtained experimental data of load-displacement, engineering stress-strain and true stress-strain curves.

3.2 Description of Specimens:

The preparation of tensile samples is a critical step in evaluating the mechanical properties of materials produced using additive manufacturing processes. The present section outlines the detailed methodology followed for developing tensile samples using the Fused Deposition Modelling (FDM) technique, adhering to the ASTM D638 standard as shown in Fig3.1. The samples are specifically designed to investigate the effects of different infill densities on mechanical performance.

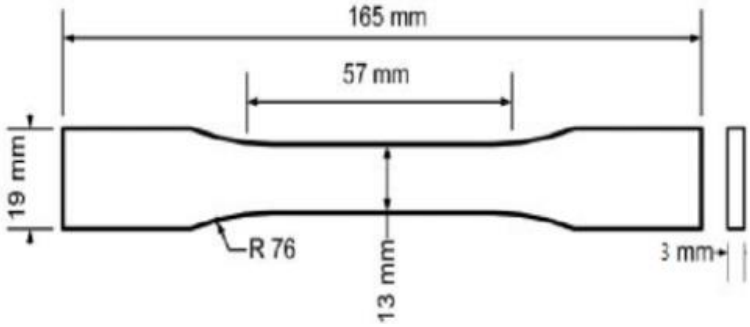

Fig 3.1: ASTM D638 Standard Tensile Specimen Dimensions

3.2.1 CAD design and STL file Conversion

The initial phase of sample development involves creating a precise CAD model of the tensile specimen, commonly referred to as a Dog-bone Sample due to its shape. The CAD model is designed in **SolidWorks** according to the ASTM D638 standard specifications to ensure consistency and comparability of results. Once the design is finalized, the CAD file is converted into an STL format, which is compatible with 3D printing software.

(a)

(b)

Fig 3.2: Prepared tensile sample CAD drawing

(a) front view and (b) Oblique view

3.2.2 Slicing and G-Code Generation

The STL file is imported into **Ideamaker** slicing software shown in Fig 3.4, where it is sliced into layers to generate the G-code. The G-code contains the specific instructions for the FDM printer, including the layer height, print speed, and infill pattern. In this study, three different infill densities (25%, 50%, and 100%) and Honeycomb infill structures are set to evaluate their impact on the tensile properties. Each infill density requires a separate slicing process to adjust the internal structure of the sample accordingly.

After creating a 3D CAD model in SolidWorks it is exported as an STL file, representing the object's surface as a mesh of triangles. IdeaMaker imports the STL, slices it into horizontal layers, and generates G-code. This code contains precise instructions for the 3D printer's movements, including extruder actions, to build the object layer by layer.

Using the generated G-code, the standard tensile samples are fabricated with PLA in **Raise 3D E2** FDM based 3D printer which can be seen in Fig 3.3. The printing parameters, such as nozzle temperature, bed temperature, and extrusion speed, are carefully controlled to ensure optimal print quality.

Fig 3.3: FDM printer used for producing test specimens

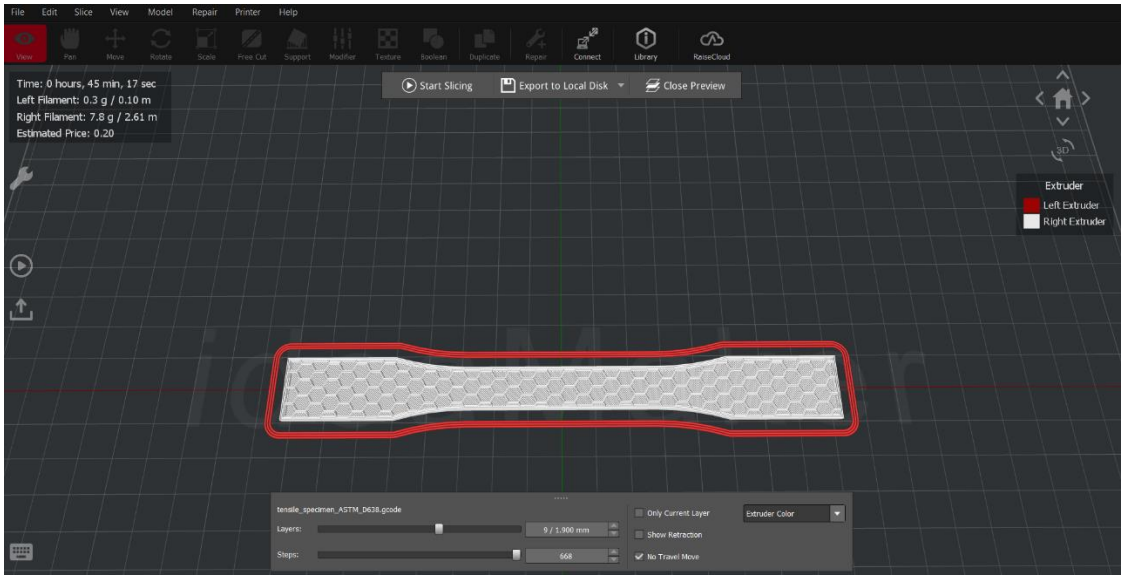

Fig 3.4: Interface of IdeaMaker Software

Table 3.1: Printing Parameters used to fabricate specimens

Printing parameters	Values
Layer thickness	0.2 mm
Printing temperature	205^0 C
Bed temperature	55^0 C
Printing Speed	60 mm/s
Infill density	25,50,100%
Infill pattern	Honeycomb
Platform adhesion	Skirt (ASTM D638), Raft (ASTM E647)
Wall thickness	0.3 mm
Top and bottom layer thickness	0.8 mm
Cooling fan speed	100 RPM
Retraction Speed	40 mm/s

After printing, the samples undergo post-processing steps to remove support structures and ensure smooth surfaces. The samples are then inspected for any defects or inconsistencies that

might affect the test results. Proper labelling and documentation of each sample, including the specific infill density and print parameters are used for traceability. The prepared tensile samples are conditioned according to standard testing requirements to ensure uniformity. Before conducting the tensile tests, the samples are measured to verify their dimensions conform to the ASTM D638 specifications. Any deviations are noted and corrected if needed.

(a)

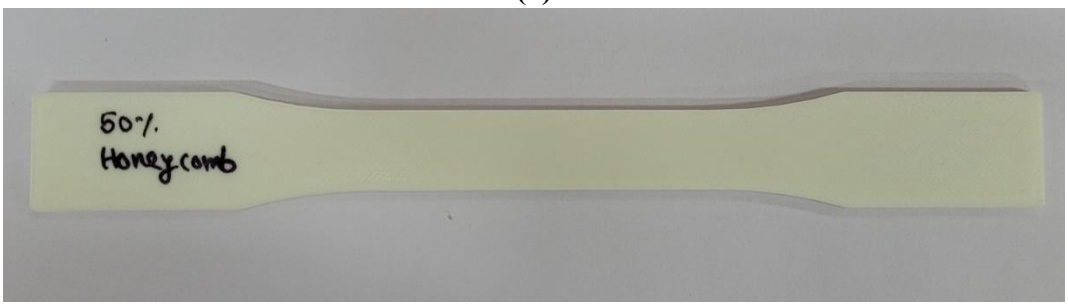

(b)

(c)

Fig 3.5: PLA tensile specimen with honeycome infill pattern

(a) 25% (b) 50% infill and (c) 100% (solid fill) infill density

The meticulous development of tensile samples is essential for accurate and reliable mechanical testing. By following a standardized procedure, this study aims to ensure that the

tensile properties of FDM-printed samples with varying infill densities are thoroughly evaluated, contributing valuable insights into the structural integrity and performance of additively manufactured materials.

3.3 Experimental Details:

All uniaxial tensile tests were carried out for the three different PLA tensile specimens having honeycomb infill pattern with each having infill density of 25%, 50%, 100% respectively in accordance with the ASTM D638 standard. All the tensile tests have been conducted on a servo-hydraulic Instron Universal Testing machine that has been depicted in Fig. 3.6, which has a capacity of 100 kN. Prior to conducting the tests, the length and thickness of the gauge section for each specimen were meticulously measured. The length and thickness found for the gauge section are 57 mm and 3 mm respectively.

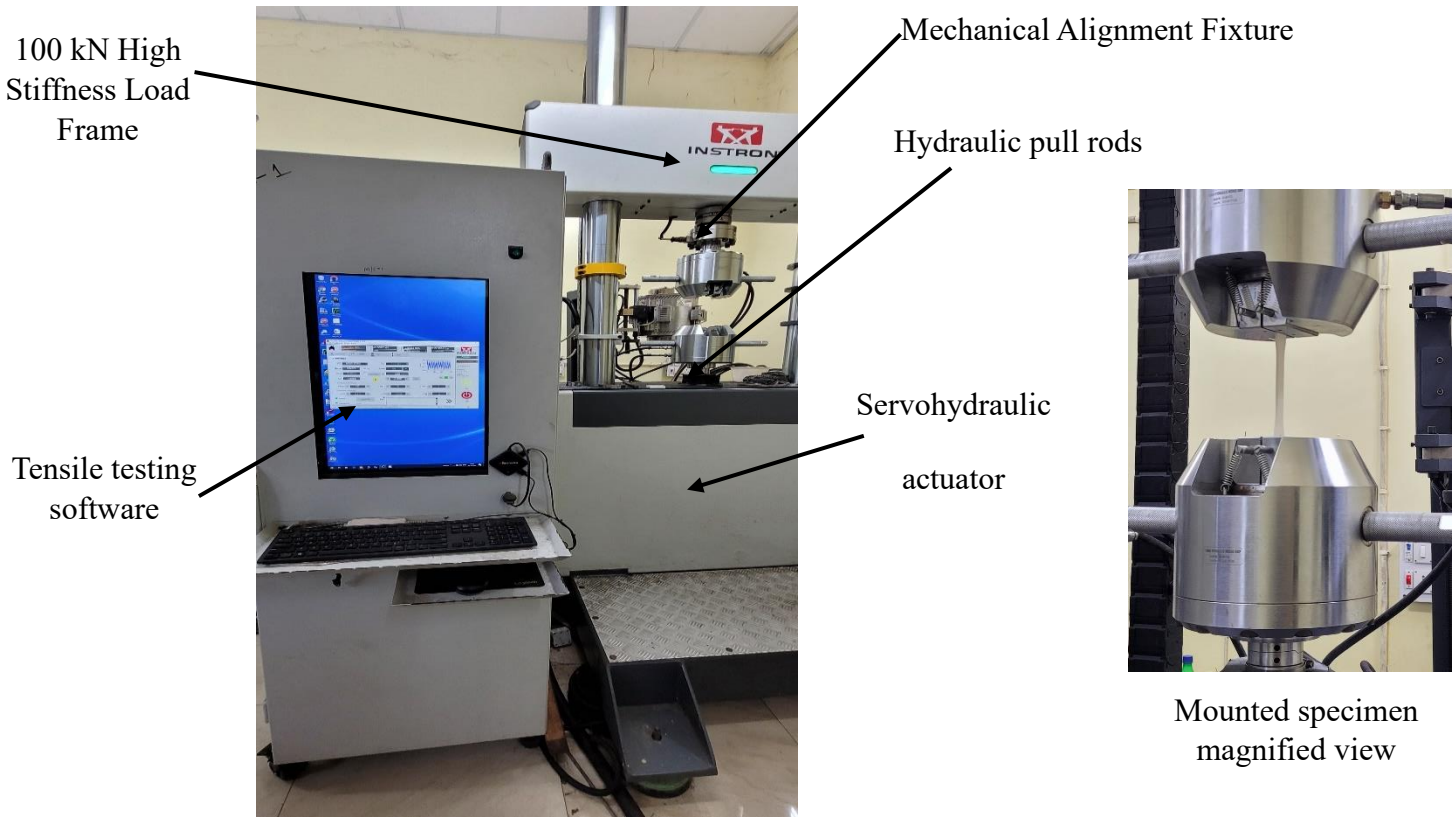

Fig 3.6: INSTRON servo-hydraulic Universal Testing machine used for tensile test

The specimens were securely clamped between the static grips of the alignment device, ensuring that the top surfaces and bottom ends were firmly held in place. An extensometer was employed to precisely measure the strain at the uniform cross-section of the specimens. This extensometer has a gauge length of 25 mm, having least count 0.01mm, a travel range of ±5 mm, allowing for accurate strain measurements. All tests were performed in displacement control mode, with $0.001s^{-1}$ strain rate, the strain rate is kept constant so that only effect of varying infill density can be observed on tensile strength of PLA material. Corresponding displacement rate has been calculated by multiplying gauge length (57 mm) with strain rate ($0.001\ s^{-1)}$ to get a value of 0.057 mm/s. The tests have been carried out in room temperature.

Table 3.2: Summary of test matrix

Specimen no.	Infill density (%)	Strain rate (s^{-1})	Gauge length (mm)	Displacement rate (mm/s)
1	25	0.001	57	0.057
2	50	0.001	57	0.057
3	100	0.001	57	0.057

3.4 Experimental Results and Discussion

The Tensile Tests have been carried out for the three PLA specimens having honeycomb infill pattern with 25%, 50% and 100% infill density. From the tests the output is generated from three sensors of the UTM namely load cell, actuator and extensometer. The raw data generated from these sensors are applied load and displacement. Load-Displacement graphs of all the three specimens are given in Fig 3.7, 3.8 and 3.9. From the Load-Displacement graphs Engineering Stress and Strain, True Stress and True Strain, and all other tensile properties are calculated. To calculate Young's modulus, tensile stress- strain is plotted at the

elastic or linear region. In the elastic region of the curve, the initial slope is declared as the Young's modulus with proportional to temperature and strain rate condition. The slope is considered for strain range in between 0.0001 to 0.001. Yield point is selected here 0.2 percent of the offset line in strain axis that cuts the tensile stress strain plot. The stress value for the yield point is considered as the material's yield strength. The Ultimate strength in tensile stress-strain plot is considered as the maximum tensile stress in the test for every temperature and strain rate. Percent elongation is the amount that a material stretches before it breaks, expressed as a percentage of its original length. Elongation is calculated by dividing the change in length of a material sample by its original length and then multiplying by 100 to get a percentage. Engineering Stress-Strain graphs for the specimens are given in Fig 3.10, 3.11 and 3.12. True Stress-Strain data is generated after test in software from the instantaneous cross section and deformation recorded. True Stress-Strain graphs are shown in Fig 3.13, 3.14 and 3.15. The fractured specimens are shown in Fig 3.16 after Table 3.2.

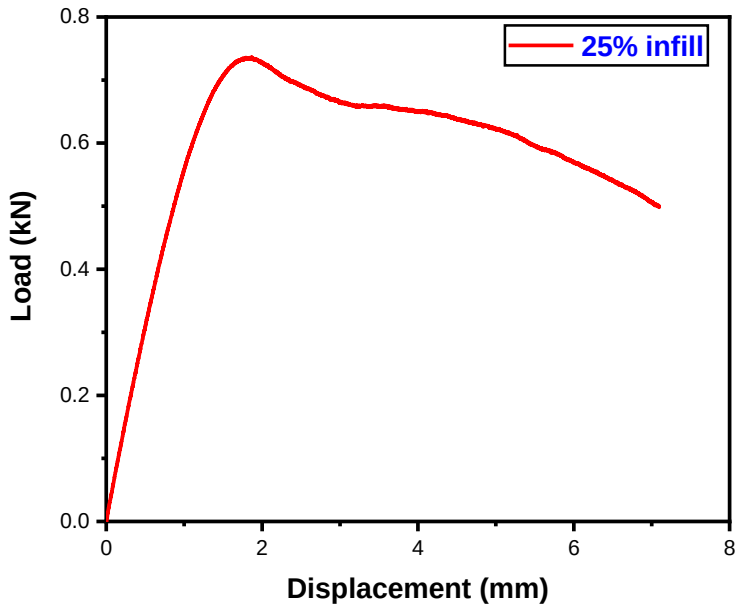

Fig 3.7: Load-Displacement graph for 25% infilled PLA specimen having Honeycomb infill pattern

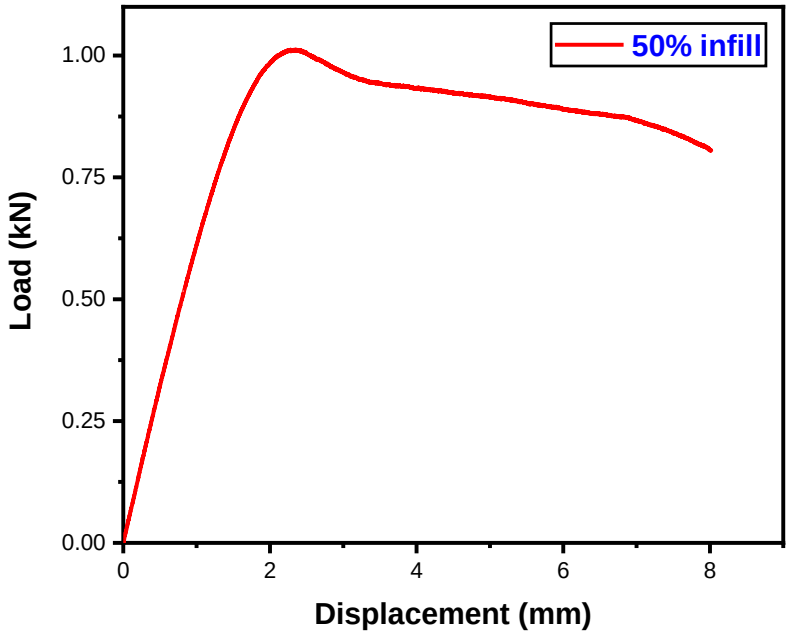

Fig 3.8: Load-Displacement graph for 50% infilled PLA specimen having Honeycomb infill pattern

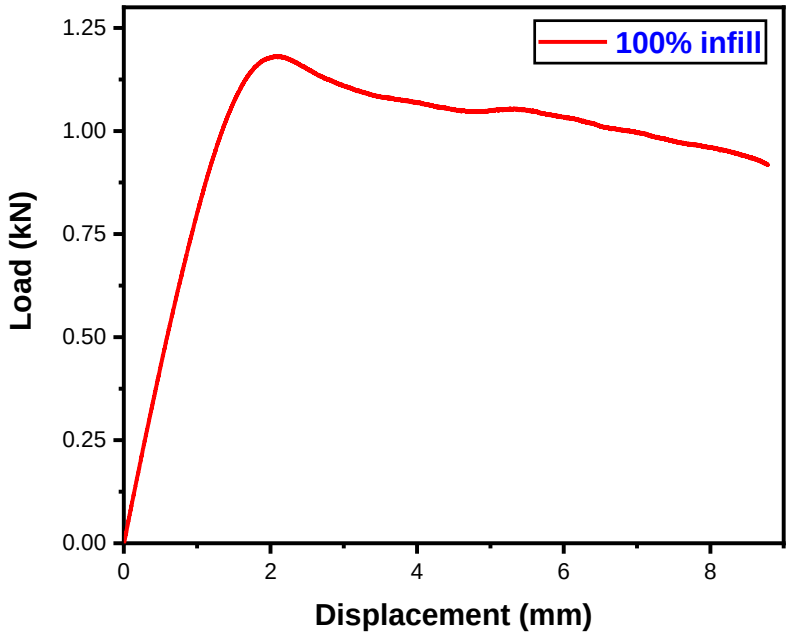

Fig 3.9: Load-Displacement graph for 100% Solid fill PLA specimen

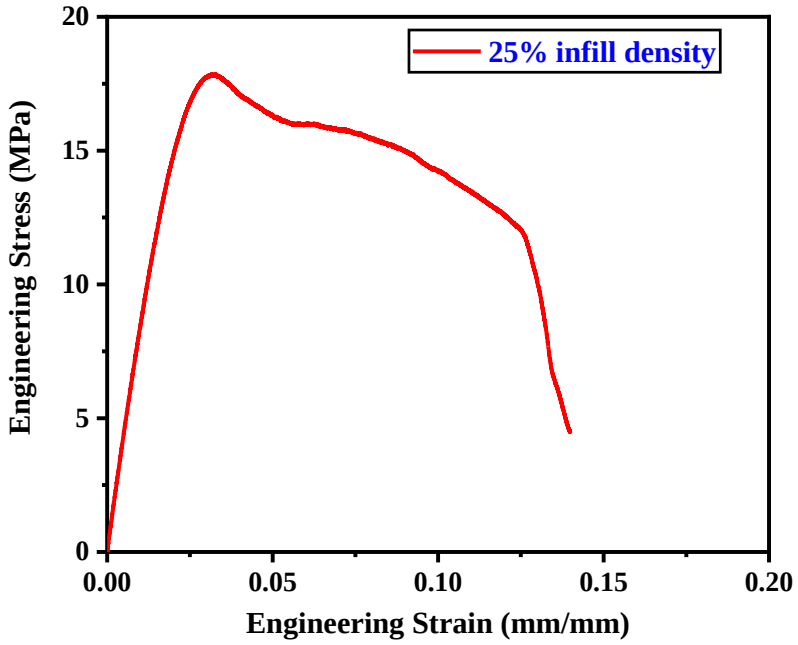

Fig 3.10: Engineering stress vs. engineering strain curve for 25% infill PLA material.

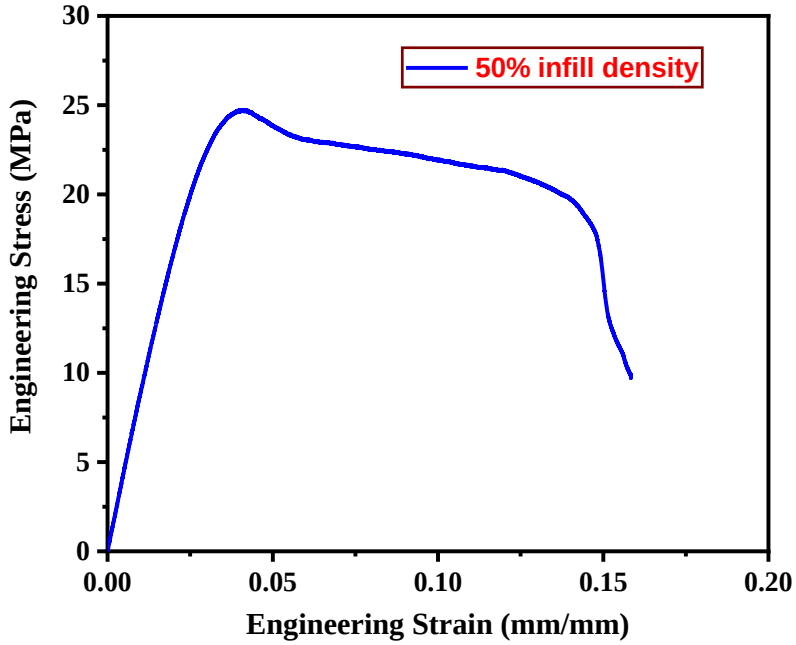

Fig 3.11: Engineering stress vs. engineering strain curve for 50% infill PLA material.

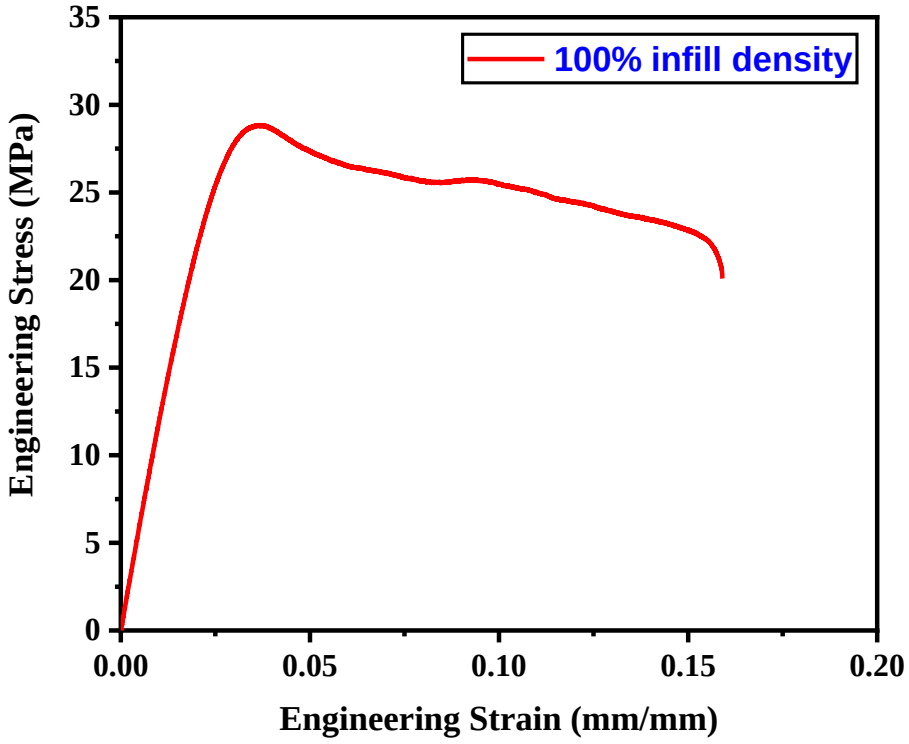

Fig 3.12: Engineering stress vs. engineering strain curve for 100% infill PLA material.

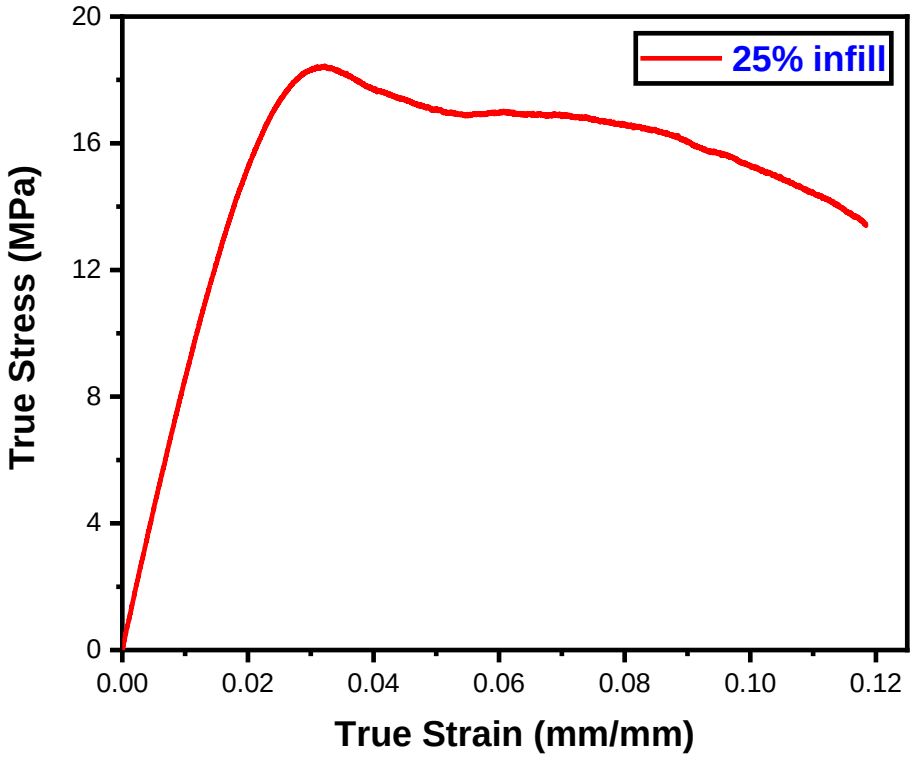

Fig 3.13: True stress vs. True strain curve for 25% infill PLA material.

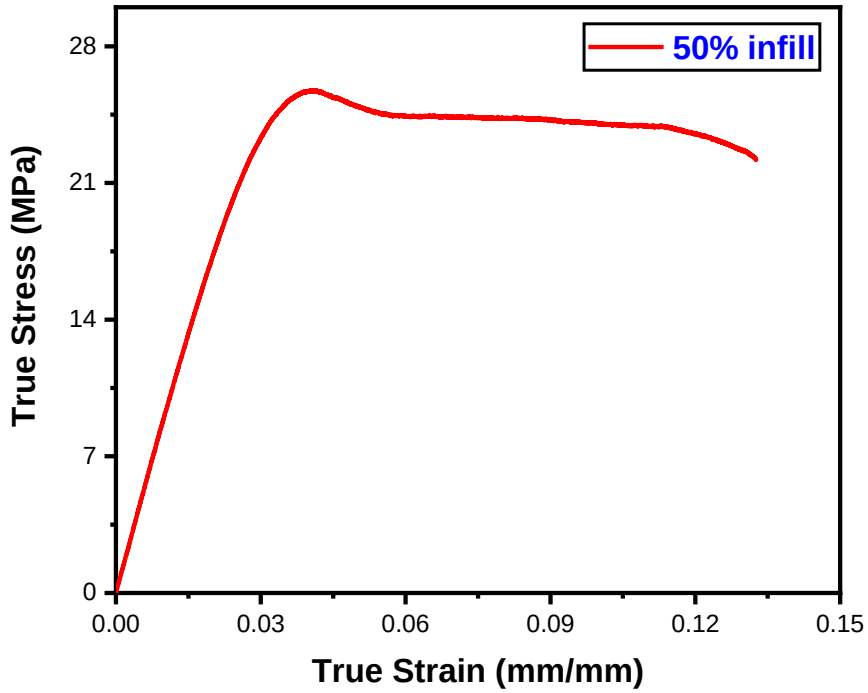

Fig 3.14: True stress vs. True strain curve for 50% infill PLA material.

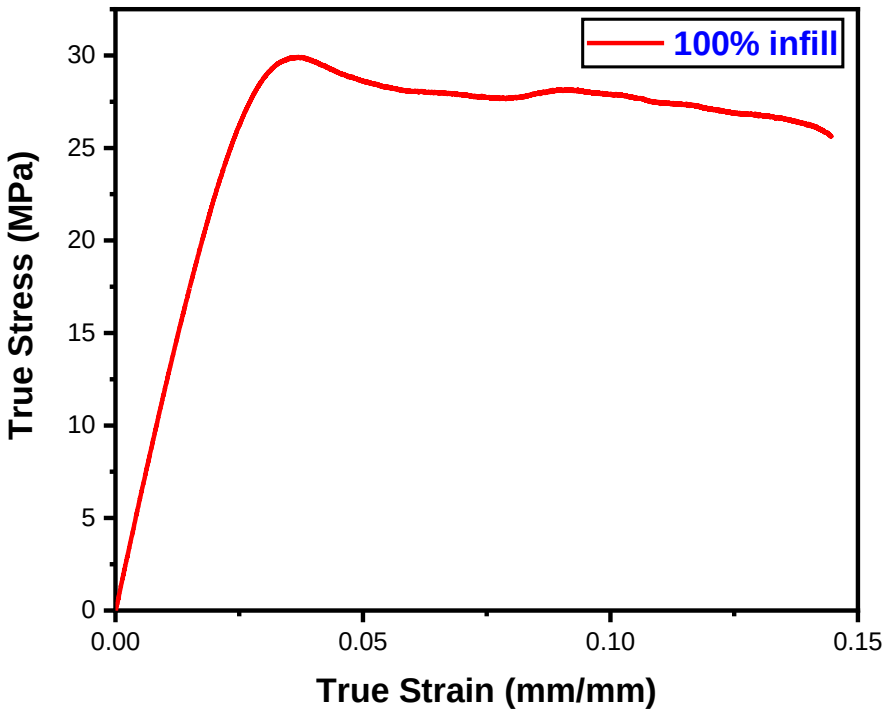

Fig 3.15: True stress vs. True strain curve for 100% infill PLA material.

Table 3.3: Tensile Test Results

Infill Density (in percentage)	Young's Modulus (GPa)	Yield Stress (MPa)	Ultimate Stress (MPa)	Percentage of Elongation
25	0.916	12.05	17.864	14.79
50	0.953	18.182	24.72	15.837
100	1.253	19.878	28.852	15.939

(a)

(b)

(c)

Fig 3.16: Fractured PLA tensile specimen having

(a) 25%. (b) 50% and (c) 100% infill density

3.4.1 Comparison study on tensile properties of 25%, 50% and 100% infill PLA material

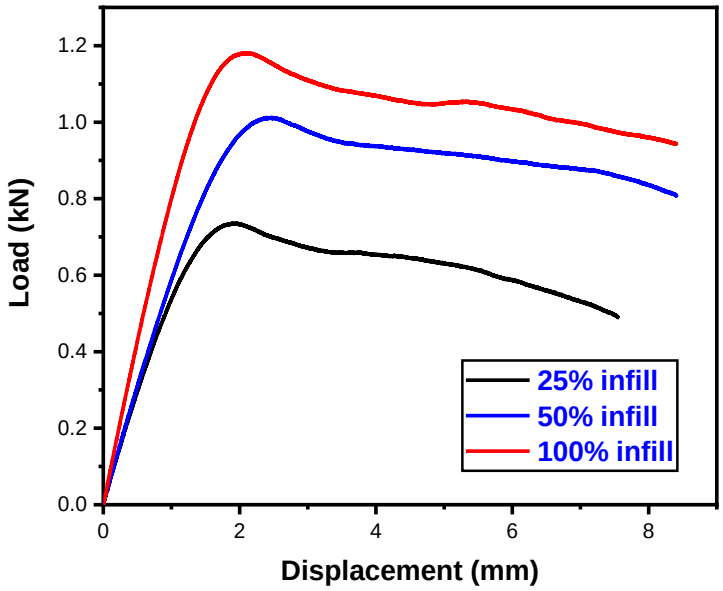

Fig 3.17: Comparison curve of Load vs. Displacement of 25%, 50% and 100% infill PLA specimen

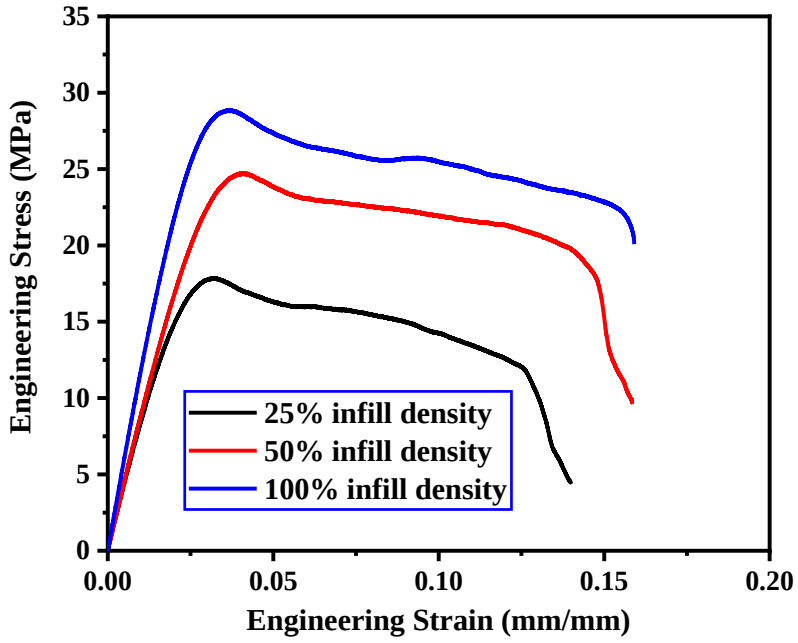

Fig 3.18: Comparison curve of Engineering Stress vs. Engineering Strain of 25%, 50% and 100% infill PLA specimen

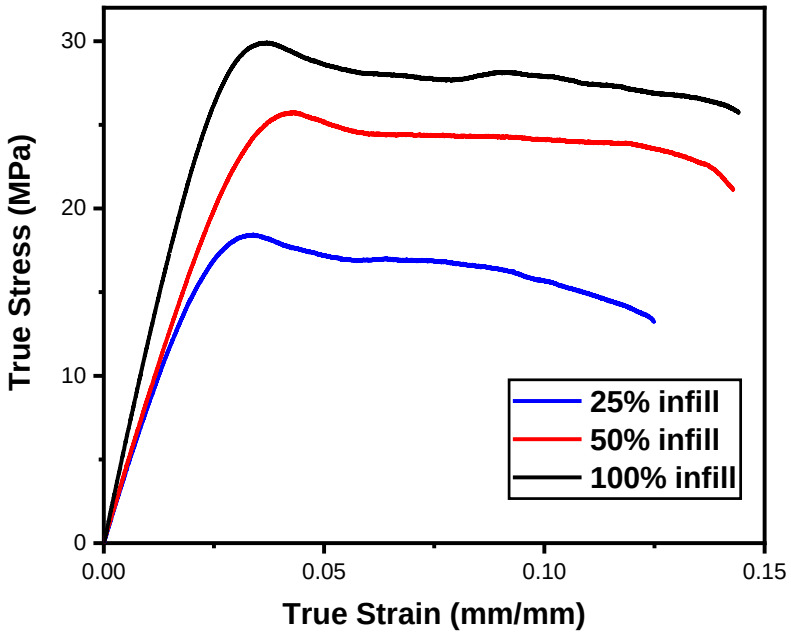

Fig 3.19: Comparison curve of True Stress vs. True Strain of 25%, 50% and 100% infill PLA specimen

From the above load-displacement comparison curve in Fig 3.17 below mentioned points can be deduced.

- The load bearing capability is maximum for 100% solid fill specimen and lowest is for 25% infilled specimens.
- Displacement before failure is quite similar for 50% and 100% infilled specimens but 25% infilled specimen shows more displacement before failure.

From the above engineering stress-strain curve in Fig 3.18 below mentioned points can be deduced.

- Yield Stress of the PLA material varies with the changing infill density, it is highest for 100% infill density and lowest for 25% infill density which can be predicted as infill density is a parameter of mass present in the specimen.
- It can be observed that the yield stress varies much more for in 50% infill specimen with respect to 25% infill specimen, whereas the change is less when 100% infill

specimen is compared to 50% infill specimen.

- The ultimate stress also follows same trend like yield stress, minimum for 25% infill specimen and it goes higher as infill density is increased.
- Being a property of material, the Young's Modulus doesn't change much in case of 25% and 50% specimens but it increases when the infill density is 100%. It can be interpreted that Young's Modulus is different for specimens having solid fill and hollow fill.
- All the specimens show significant amount of plastic strain before it fails, signifying ductile nature of PLA material.
- The total elongation exhibited by the PLA tensile specimen increases gradually with increasing infill density.

3.5 Conclusions:

By analysing results of the tensile tests below mentioned points can be made

- The yield strength of 50% infilled PLA specimen is 50.89 % more that of 25% infilled PLA specimen and 17.01% lesser than 100% solid fill PLA specimen.
- The ultimate strength of 50% infilled PLA specimen is 38.38 % more that of 25% infilled PLA specimen and 16.72 % lesser than 100% solid fill PLA specimen.
- The percentage elongation of 50% infilled PLA specimen is 7.08% more that of 25% infilled PLA specimen and 0.64 % lesser than 100% solid fill PLA specimen.
- All the specimen shows considerable amount of deformation before failure, exhibiting ductile nature of PLA material.

Chapter 4: FCGR Testing

4.1 Introduction:

This chapter details the experimental procedure for fatigue crack growth rate (FCGR) testing of 3D printed polylactic acid (PLA) specimens. It outlines the steps involved, including specimen preparation, fatigue pre-cracking, crack size measurement using the unloading compliance method, and the FCGR testing procedure itself. The chapter also discusses the analysis of experimental results to determine parameters like the Paris constant, Paris exponent, and threshold stress intensity factor (ΔK_{TH}).

4.2 Description of the Specimens:

Compact Tension (CT) specimens are developed, following ASTM E647-15[67] Standard for FCGR testing. Here full-size CT specimen following ASTM E647-15 specifications shown in Fig 4.1 has been developed using FDM printer with 100% infill density and the material used is **Polylactic Acid (PLA).** Initially CAD drawing is prepared in accordance with the standard as can be seen in Fig 4.2 and Fig 4.3. The CAD drawing is then converted to STL file for G-Code preparation. Following G-code preparation the FDM printer

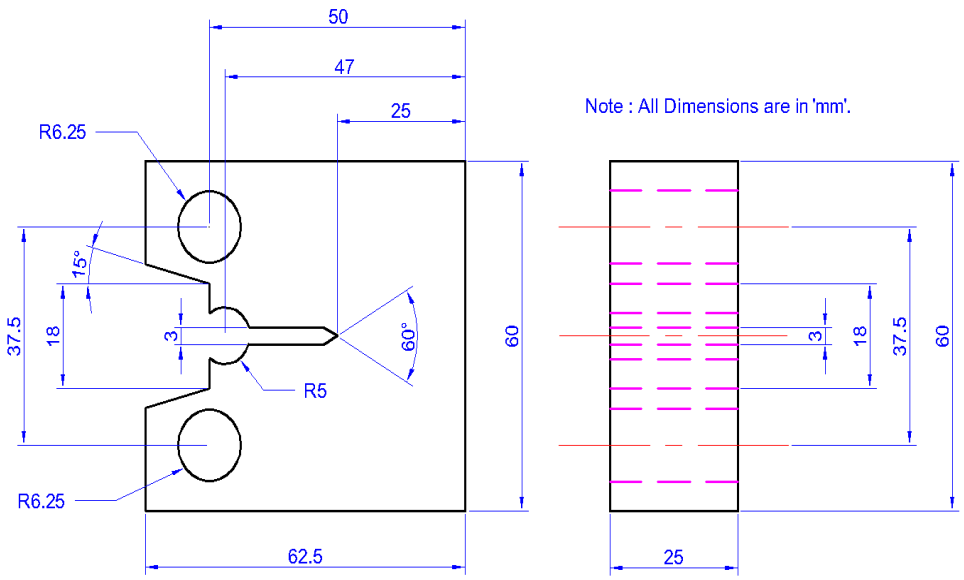

Fig 4.1: Full Size CT specimen Drawing following ASTM E647 Standard

is set-up for printing and all the parameters are checked thoroughly. After printing is completed, the specimen is taken out from the printer and proper labelling was done to avoid mismatch. The printed specimen is given in Fig 4.4.

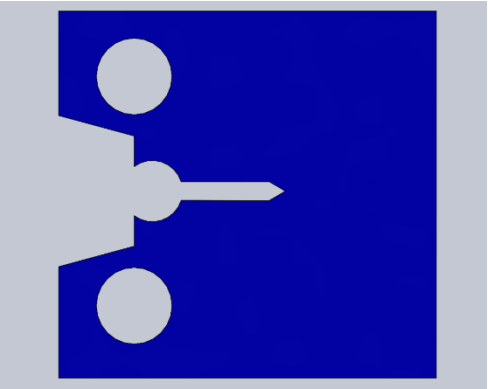

Fig 4.2: CT Specimen CAD model front view

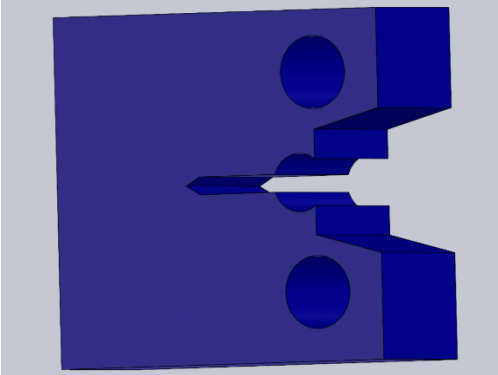

Fig 4.3: CT Specimen CAD model oblique view

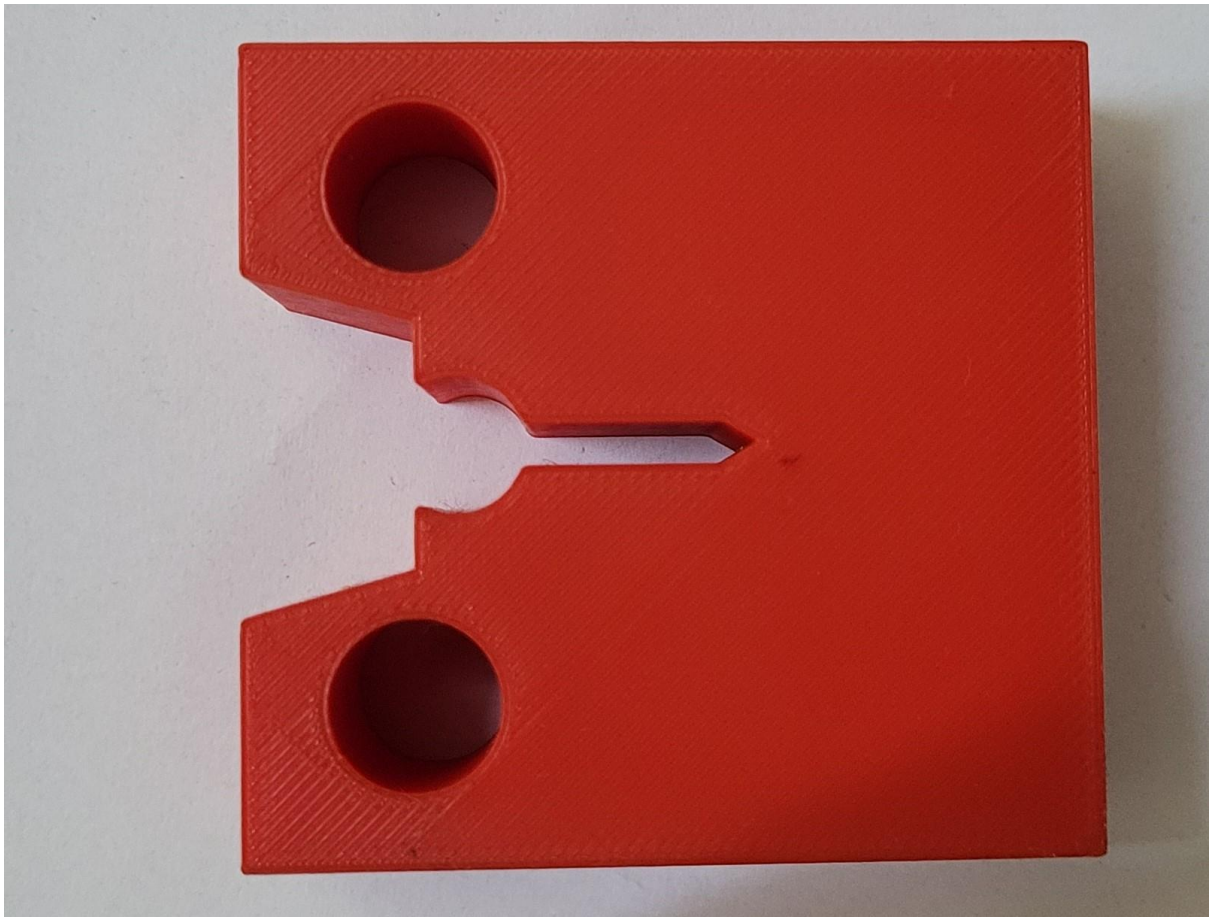

Fig 4.4: FDM printed CT specimen

After preparing all the specimens, they are taken for tests. Total 3 tests with each having different infill density are conducted following ASTM guidelines.

4.3 Experimental details:

4.3.1 Fatigue pre-cracking:

Before conducting FCGR testing a fatigue pre-cracking is performed on the specimen to obtain a sharpened crack of desired size and straightness which eliminates the effect of a machined starter notch in specimen K-calibration.

- Before fatigue pre-cracking the notch length was measured as 25mm ($a/W = 0.5$)
- As per ASTM E647-15, the fatigue pre-crack length should not be less than 0.1B, h or 1 mm whichever is greater. So, to confirm 'a/W' ratio as 0.55 before FCGR testing fatigue pre-cracking was conducted so that the final notch length could reach up to 27.5 mm ($a/W = 0.55$) as per ASTM E647-15.
- Fatigue pre-cracking was conducted in load control mode.
- During pre-cracking the K_{max} should be controlled with stepped down loading method so that the final K_{max} does not exceed the value of initial K_{max} during FCGR testing.
- To avoid increase in K_{max} & ΔK with increase in crack length as in the case of constant load cycle during fatigue pre-cracking, load range was stepped down during pre-cracking as per ASTM E647-15.

$$K_{max} = \frac{P_{max}}{B\sqrt{W}} \frac{2+\alpha}{(1-\alpha)^{1.5}} (0.886 + 4.64\alpha - 13.32\alpha^2 + 14.72\alpha^3 - 5.64\alpha^4) \qquad (4.1)$$

Where, $\alpha = \frac{a}{W}$

- The initial value of maximum fatigue load was adopted as 40% of P_f according to ASTM E647-15. Where,

$$P_f = \frac{0.4Bb_0^2\sigma_{FS}}{(2W+a_0)}, \quad Where \ \sigma_{FS} = \frac{(\sigma_{YS}+\sigma_{TS})}{2} \qquad (4.2)$$

4.3.2 Crack Size Measurement using Unloading Compliance Method

The unloading compliance method is used for measuring crack growth in the FCGR testing of ductile materials. The method involves partially unloading and then reloading a specimen at specified intervals during the test. From the unloading slopes, which tend to be linear and independent of prior plastic deformation, the crack length is estimated using analytical elastic compliance relationships. Crack size can be measured with elastic compliance technique on compact specimen through crack opening displacement measured along the load line displacement. The load line displacement (Δ) is composed of two components, i.e. Δ_{nc} and Δ_c as shown in the following equation.

$$\Delta = \Delta_{nc} + \Delta_c \tag{4.3}$$

Where Δ_{nc} is the load line displacement in absence of crack and Δ_c is the additional displacement due to crack. For compact specimen $\Delta_{nc} = 0$ because it is measured at the crack mouth. Now to measure the crack length a fifth order polynomial was established as per ASTM E1820 between normalized crack length (a/W) and unloading compliance as shown in the following equations.

$$\frac{a}{W} = 1.00196 - 4.06319U_{LL} + 11.242U_{LL}^2 - 106.043U_{LL}^3 + 464.335U_{LL}^4 - 650.677U_{LL}^5 \tag{4.4}$$

where,

$U_{LL} = \frac{1}{1+\sqrt{Z_{LL}}}$ and $Z_{LL} = \frac{BE\Delta}{P}$

B = Specimen thickness (For side grooved specimen, $B_e = B - \frac{(B-B_N)^2}{B}$)

B_N = Net thickness, E = Young's Modulus and Δ/P = Compliance.

4.3.3 FCGR Testing

Instead of using increasing ΔK, this FCGR test employs a decreasing ΔK approach. It starts with ΔK and K_{max} values that are at least as high as the final values used during fatigue

pre-cracking. As the crack grows larger, the forces are gradually reduced until the desired minimum crack growth rate or ΔK value is reached.

The tests were conducted using a 25 kN INSTRON servo-hydraulic universal testing machine. An external COD gauge is attached to the CT specimen for accurate measurement of crack. The COD gauge is attached in load line of CT specimen and the gauge length of the CT specimen was 5mm. Before starting the test, the load cell and the COD gauge is calibrated using the shunt value of respective sensors. The test setup is given below in Fig 4.5 also the sinusoidal loading applied to the specimen is illustrated in Fig 4.6.

It's important to note that ASTM E647 discourages using decreasing ΔK cycles for FCGR measurements when the crack growth rate surpasses 10^{-8} m/cycle. Throughout this test, the force is lowered by decreasing the load amplitude at specific crack size intervals.

- The procedure is controlled with normalized K gradient (C) as mentioned above which should be greater than or equal to -0.08 mm^{-1} as shown in the following equation.

$$C = \frac{1}{\Delta K}\frac{d\Delta K}{da} > -0.08\, mm^{-1} \tag{4.5}$$

- Integrating the above differential equation with suitable constants we get,

$$\Delta K = \Delta K_0 \exp\left[C(a - a_0)\right] \tag{4.6}$$

  Where, ΔK_0 and a_0 are the initial ΔK and crack size respectively.

- During test procedure the force ratio (R) and normalized K gradient (C) was maintained at constant value of 0.1 and -0.08 respectively.
- The test was started with an initial ΔK (ΔK_0) value of 1.37 MPa√m with a corresponding initial crack length (a_0) 27.5 mm.
- The cyclic frequency was maintained at 15 Hz.

Fig 4.5: FCGR test in progress

Fig 4.6: Sinusoidal loading applied during testing

4.4 Experimental Results and Discussion:

- The rate of crack growth is calculated using the secant or incremental polynomial method based on the collected data on crack size and the number of cycles that have passed. As per ASTM E647-15, while computing the crack growth rate for decreasing ΔK test the secant method is recommended due to force shedding in decremented step.
- The secant method involves the point-to-point slope determination on **a** vs **N** curve as shown in the following equation. As $\frac{da}{dN}$ is computed as an average over the range of a_i to a_{i+1}, the average crack size which is used to compute ΔK is $\frac{a_{i+1}+a_i}{2}$.
- As shown in the below schematic Fig 4.7, the linear profile represented in Log $\frac{da}{dN}$ vs Log ΔK curve is adopted for evaluating the Paris constant and exponent. Hence the slope of the linear profile represents the exponent and the intercept represents the Paris constant as shown in the following equation

$$\frac{\mathrm{da}}{\mathrm{dN}} = \mathrm{C}\Delta\mathrm{K}^{\mathrm{m}} \tag{4.7}$$

$$\mathrm{Log}\frac{\mathrm{da}}{\mathrm{dN}} = \mathrm{mLog}\Delta\mathrm{K} + \mathrm{LogC} \tag{4.8}$$

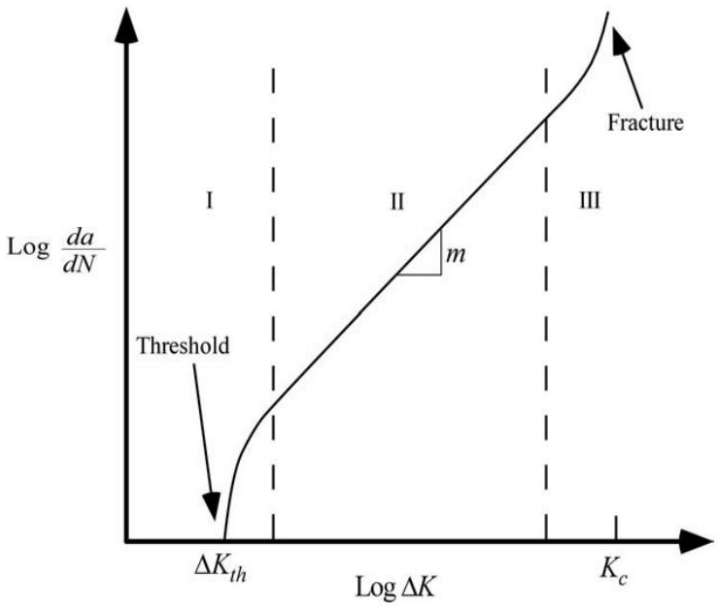

Fig 4.7: Schematic representation of FCGR behaviour for any material.

- Within the range of crack growth rate between 10^{-9} to 10^{-10} m/cycle at least five points are selected from the Log $\frac{da}{dN}$ vs. Log ΔK curve and the obtained best fit straight-line equation from those points is used to evaluate the ΔK_{th} comparable to the crack growth rate of 10^{-10} m/cycle.

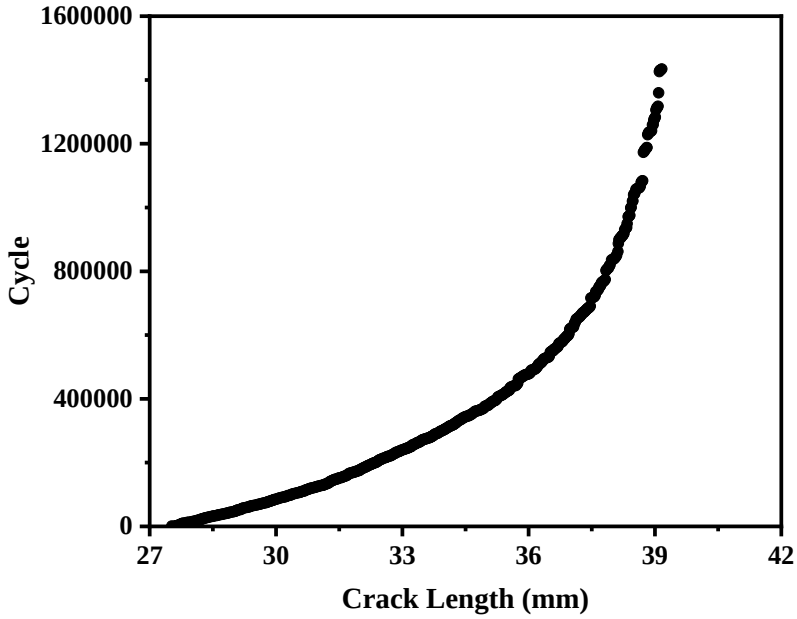

Fig 4.8: Crack length(a) vs. Cycle(N) curve for 100% infilled PLA material

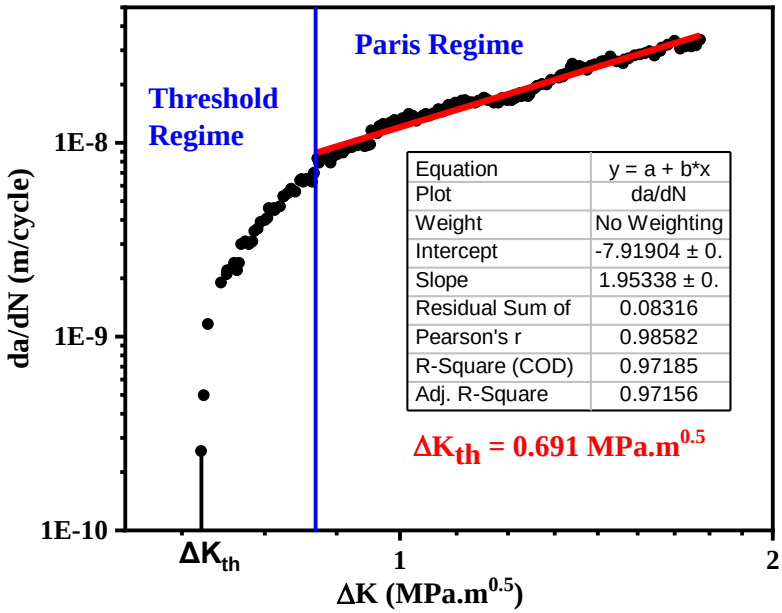

Fig 4.9: $\frac{da}{dN}$ vs. ΔK curve for 100% infilled PLA material

Initially the intention of the research was to find the effect of infill density with fatigue crack growth rate properties such as Paris constant, Paris exponent and Threshold stress intensity factor. During testing of specimens having 25% and 50% infill density the test stopped just after the first loading-unloading cycle to measure the crack propagation. The reason behind this abrupt stopping of test can is the intentional porosities present inside the specimen as infill density. The COD gauge after one loading cycle faces the voids present in the specimen causing the Universal Testing Machine to malfunction. Thus, only solid fill CT specimen's FCGR test is carried out.

After completion of FCGR test, the test data was extracted from the system i.e. a vs N data, which is given in Fig 4.8. Post-test analysis has been carried out in ORIGIN software to find Paris constant, Paris exponent and ΔK_{th} .

Curve fitting was done to find a suitable straight line joining the scattered results in the Paris regime. The Fatigue crack growth rate curve or $\frac{da}{dN}$ vs. ΔK curve for 100% infilled PLA material curve is given in Fig 4.9.

The Paris constant(C) for PLA material found = $1.2049 \times 10^{-8} \frac{\frac{mm}{cycle}}{(Mpa\sqrt{m})^m}$

and the Paris exponent(m) found = 1.953.

The value for ΔK_{th} is found to be 0.691 MPa.m$^{0.5}$.

4.5 Conclusions

The study successfully investigated fatigue crack growth in 3D printed PLA material having 100% infill density and honeycomb infill pattern. The Paris law parameters, C = $1.2049 \times 10^{-8} \frac{\frac{mm}{cycle}}{(Mpa\sqrt{m})^m}$ and m = 1.953, and ΔK_{th} is found to be 0.691 MPa.m$^{0.5}$ were determined, providing valuable data for understanding and predicting fatigue behaviour in 3D printed PLA structures.

Chapter 5: Fracture Toughness Testing

5.1 Introduction:

The present chapter investigates the fracture toughness of 3D printed polylactic acid (PLA) material, a crucial mechanical property that characterizes a material's resistance to fracture in the presence of a crack. Building upon the fatigue crack growth rate (FCGR) testing performed in the previous chapter, this chapter employs compact tension (CT) specimens having honeycomb infill pattern with varying infill densities (25%, 50%, and 100%) to assess the material's fracture behaviour under monotonic loading. The study adheres to the ASTM E1820-13[68] standard, a widely recognized benchmark for fracture toughness testing of metals, ensuring methodological rigor and comparability of results.

Key aspects of the experimental procedure include fatigue pre-cracking of the specimens, precise crack length measurement using the unloading compliance method, and the application of the J-integral approach to quantify fracture toughness. The J-integral, a measure of the strain energy release rate at the crack tip, is used to determine both the crack initiation fracture toughness (K_{JC}) and the fracture toughness (J_{IC}). The experimental data is meticulously analysed to generate J-R curves, which depict the relationship between the J-integral and crack extension, enabling a comprehensive understanding of the material's resistance to crack growth.

By conducting fracture toughness tests on 3D printed PLA with different infill densities, this chapter aims to elucidate the impact of infill density on the material's fracture properties, providing valuable insights for optimizing the design and fabrication of 3D printed PLA components for enhanced structural integrity and reliability.

5.2 Description of the Specimen:

The specimen used for fracture toughness testing in this chapter is the same Compact Tension (CT) specimen utilized in the previous chapter for fatigue crack growth rate (FCGR)

analysis and the CAD drawing and fabricated specimen is given in chapter 4 as Fig 4.2, 4.3 and 4.4. The dimension for preparing the CT specimen according to ASTM E1820-13 is given in Fig 5.1. However, in this chapter, the focus shifts from studying crack growth under cyclic loading to evaluating the material's resistance to fracture under monotonic loading.

To produce the CT specimens, a CAD drawing was created in accordance with ASTM E1820-13 specifications. The drawing was then converted into an STL file for G-Code generation, which guided the FDM 3D printer in fabricating the specimens. Various infill densities (25%, 50%, and 100%) were employed to investigate their influence on fracture toughness. The material used for printing was Polylactic Acid (PLA).

The dimensions of the CT specimens adhere to the ASTM E1820-13 standard, ensuring comparability with established fracture toughness testing practices. The specimens have a specimen width (W) of 50 mm measured from load-line, a thickness (B) of 25 mm. The uncracked ligament length(a) is 25 mm, resulting in an a/W ratio of 0.5. Fatigue pre-cracking is performed to achieve a final notch length of 27.5 mm, corresponding to an a/W ratio of 0.55, as required by the standard.

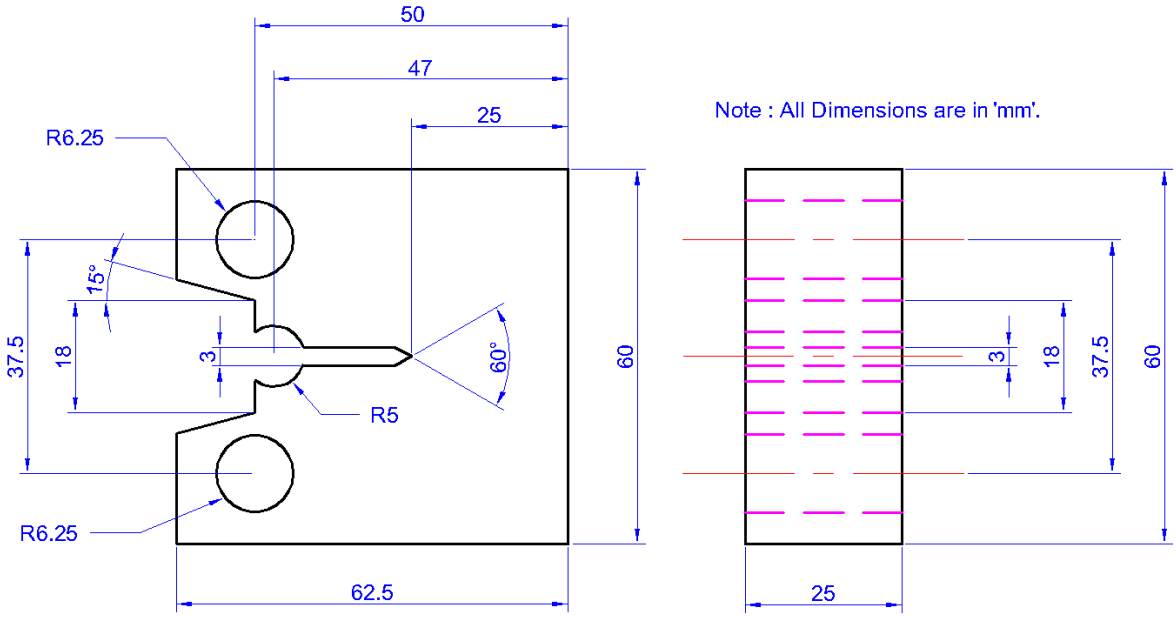

Fig 5.1: CT specimen Drawing following ASTM E1820-13

5.3 Experimental details:

The experimental details for fracture toughness testing, as guided by ASTM E1820-13, involve specific procedures to evaluate this property under varying loading conditions. The fracture toughness testing process generally includes fatigue pre-cracking, which has been explained in Chapter 4, as it adheres to ASTM E647-15 for initiating a sharp crack, followed by side-grooving and the fracture test itself to generate the J-R curve. The fracture test involves monotonically loading the prepared specimen until fracture, while carefully monitoring and recording parameters like load, displacement, and crack growth. The collected data is then used to construct the J-R curve, which illustrates the relationship between the J-integral and crack extension, offering valuable insights into the material's resistance to crack growth and aiding in determining its fracture toughness (J_{IC}). To investigate the potential impact of loading rate on fracture toughness, the tests are conducted under displacement control mode with 0.05 S^{-1} loading rates. It is important to note that the loading rate during the fracture test can significantly influence the measured J-integral value, with higher loading rates generally leading to higher J-integral values. Additionally, adherence to ASTM E1820-13 guidelines regarding temperature control, alignment, and fixture considerations is crucial for ensuring data accuracy and reliability. By meticulously following these experimental details and the comprehensive guidelines outlined in the standard, the fracture toughness testing procedure is carried out allowing for a thorough characterization of the fracture behaviours of 3D printed PLA material.

5.3.1 Fracture Testing (J-R curve)

ASTM E1820-13 describes the standard procedure for fracture testing and thereby evaluation of fracture toughness (J_{IC}) of metal. Fracture toughness is measured at the onset of ductile crack growth following the J-R resistance curve obtained from monotonically loading the specimen up to failure. Crack growth has been measured with the help of unloading

compliance method as described earlier. The test specimens were made side-grooved to 20% net depth to restrain the crack growth along the plane of symmetry for the minimization of short crack growth and to avoid shear lips or crack tunnelling as per ASTM E1820-13. At first the fatigue pre-cracking has been done on the above-mentioned side-grooved specimen following the same procedure as mentioned before but in this case the pre-crack length was maintained at 2.5 mm for all the specimens so that the a/W ratio could be fixed with 0.5. Therefore, after pre-cracking the total crack length was obtained as 27.5 mm. The objective of this test procedure is to develop a load displacement dataset to evaluate J-R curve from which the fracture toughness (J_{1c}) of a material is computed following ASTM E1820-13 standard procedure. Fig 5.2 shows the experimental setup for fracture toughness testing.

Fig 5.2: Fracture Toughness testing in progress

- The fracture toughness resistance curve procedure is used to evaluate fracture toughness using COD gauge as crack growth measuring equipment.
- This process requires an elastic unloading procedure throughout the crack extension for measuring crack growth using unloading compliance method.
- The J-R fracture tests have been conducted in displacement control mode with a loading rate of 0.01 mm/s, 0.05 mm/s, 0.075 mm/s and 0.1 mm/s.
- With the help of unloading compliance method, the initial crack length (a_0) was measured within a load range from 0.5 to 1.0 times the maximum pre-cracking load which is about 2.5 kN and thereby a provisional initial crack size was determined by averaging with ten unloading-reloading sequences.
- The data acquisition software is used to acquire data that specifies load (P), load line displacement (LLD) and crack length (a) through test application.

5.3.1.1 J_{IC} Computation

In addition to measuring load (P), load line displacement (LLD) and crack length (a), the value of J was computed through the following procedure and thereby the J-Δa curve was obtained from which the fracture toughness (J_{IC}) was determined. For computation of J with respect to crack growth (Δa), the most convenient way is to divide J into its elastic and plastic components as shown in the following equations.

$$J = J_{el} + J_{pl} \tag{5.1}$$

Where elastic component of J (J_{el}) is computed from elastic stress intensity factor K as shown in the following equation.

$$J_{el} = \frac{K^2\,(1-\nu^2)}{E} \tag{5.2}$$

For side grooved specimen the stress intensity factor is computed from the following equation, where 'B' is the gross thickness (B = 6.25 mm) and 'B_N' is the net thickness (B_N = 5 mm).

$$K = \frac{P}{\sqrt{BB_N W}} f(a/W) \tag{5.3}$$

According to ASTM E1820-13, the plastic component of J (J_{pl}) is computed from the plastic area (A_{pl}) under the load–displacement curve as shown in the following equation. Where 'η' is a dimensionless constant, 'B_N' is the net thickness and 'b_0' is the initial uncrack ligament length.

$$J_{pl} = \frac{\eta A_{pl}}{B_N b_0} \tag{5.4}$$

After obtaining the *J-Δa* curve (as shown in the schematic Fig 5.3) two exclusion lines were drawn with a slope of $M\sigma_F$ at different crack extensions of 0.15 mm and 1.5 mm respectively. Where σ_F is the flow stress defined by averaging a material's yield and ultimate strength. The value of $'M'$ here is taken as 2 according to ASTM E-1820 standard. All those data points that fall within the exclusion lines were fitted to a power law regression. The regression is a power law in the form of

$$J = C_1(\Delta a)^{C_2} \tag{5.5}$$

Where, C_1 and C_2 are constants coefficient and exponent respectively for regressions and are not based on measurements. After regression analysis, considering a crack extension of 0.2 mm, an offset line is drawn taking the same slope of $M\sigma_F$. The point at which this offset line will intersect the power law fitting curve, that intersecting points define as J_Q and Δa_Q as shown in the following Fig. 3. Qualification of J_Q as J_{IC}, a size independent value of elastic-plastic fracture toughness (J_{IC}) has been considered, if:

i. Thickness, $B > 25\frac{J_Q}{\sigma_Y}$,

ii. Initial uncrack ligament length, $b_0 > 25\frac{J_Q}{\sigma_Y}$,

iii. The slope of the power law regression line, $\frac{dJ}{da}$, evaluated at Δa_Q is less than σ_Y.

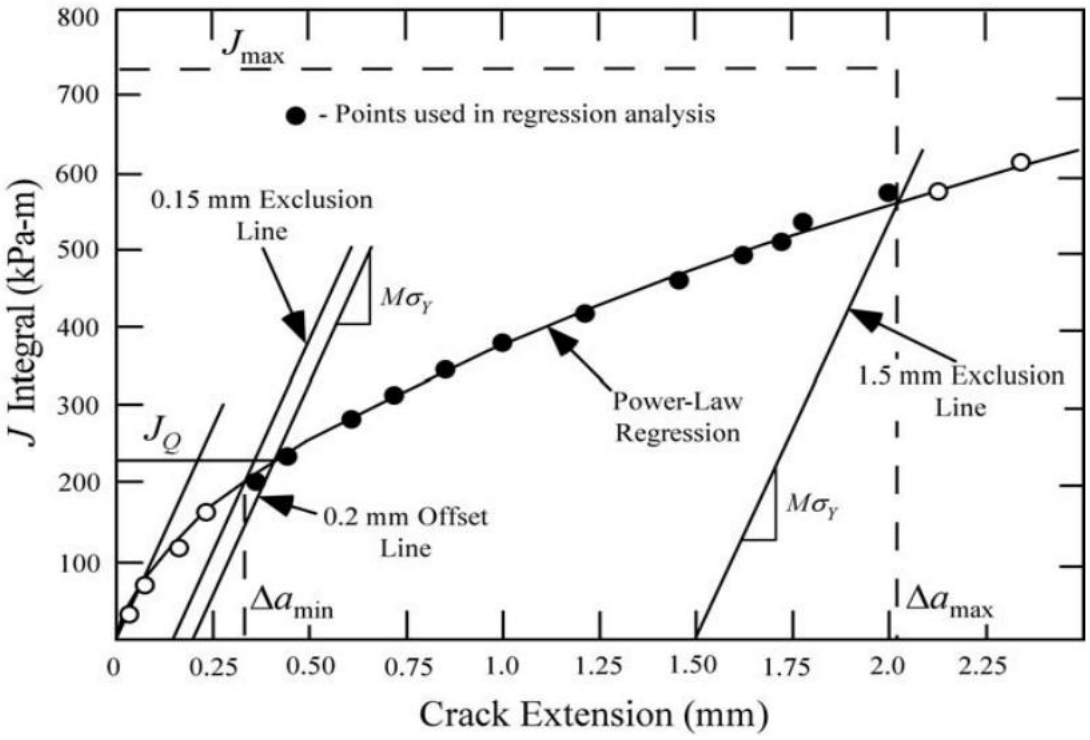

Fig 5.3: Schematic representation for determination of J_{IC} from J-Δa curve [69]

5.3.2 Crack Initiation Fracture Toughness (J_{1c} to K_{JC}):

For ductile–brittle transition fracture, the toughness demonstrates much greater variability due to the ‘‘weakest link’’ failure mechanism that initiates cleavage in these materials. In some cases, the cleavage initiation toughness can be defined in terms of a critical elastic K_C, but other tests at the same temperature likely require the use of the elastic–plastic J-integral to accurately define the cleavage initiation. For each specimen, first measured as J_C, the J-integral at the onset of cleavage, and subsequently converted to K_{JC}. From a J–R curve, the characteristic values of elastic–plastic fracture mechanics (EPFM) are deduced generally. One of significant parameters is the plane strain initiation toughness J_{IC} that provides a measure of crack growth resistance near the onset of stable crack growth for Mode-I cracks. Since, it is difficult to define the instant of crack initiation in ductile metals, different definition of initiation toughness is used in different test standards, as discussed by Roos and Eisele [70]. ASTM E1820-13 adopts an engineering definition of J_{IC} at the intersection of a 0.2-mm offset construction line and the J–R curve, as shown by J_Q in Fig 5.3 This figure illustrates a typical

construction procedure used to evaluate J_{IC} as specified in ASTM E1820-13. Experiments showed that J_{IC} is nearly a geometry-independent fracture parameter over the range of C(T) specimen sizes allowed by E1820-13. Because the J concept applies equally well to structures failing in elastic conditions and in fully-plastic conditions, K_{JC} is related to J_{IC} in the following relationship:

$$K_{JC} = \sqrt{J_{IC}E} \tag{5.6}$$

Note that Begley and Landes related J_{IC} to K_{IC} in Eq. (13), recognizing that linear elastic fracture mechanics is a special case of non-linear elastic fracture mechanics. However, since J_{IC} and K_{IC} are defined differently by ASTM E1820-13 and E399[71], respectively, a relationship between them is not possible. Accordingly, as is done in E1820-13, we use K_{JC} here when the initiation fracture toughness is measured using J_{IC} and the E1820-13 method, and K_{IC} when the initiation fracture toughness is measured using the E399 method.

5.4 Experimental Results:

The fracture toughness tests, conducted in accordance with ASTM E1820-13, yielded valuable data that elucidates the fracture behaviour of 3D printed PLA specimens with varying infill densities. The load-displacement curves that is Fig 5.4, Fig 5.5 and Fig 5.6 for 25%, 50% and 100% infill density PLA fracture specimen having Honeycomb infill pattern and the corresponding J-R curves constructed from the load displacement curve using exclusion lines, offset line and subsequent J-R curve is constructed which is given below as Fig 5.7, Fig 5.8 and Fig 5.9 for 25%, 50% and 100% infill density PLA fracture specimen. This meticulously generated results from the experimental data, offer a quantitative assessment of the material's resistance to crack initiation and propagation. Table 5.1 shows the results found from the fracture toughness test conducted for different infill density PLA specimens also from the Youngs Modulus results in chapter 3 crack initiation fracture toughness is also mentioned in the Table for 25%, 50% and 100% infill densities specimen having Honeycomb infill pattern.

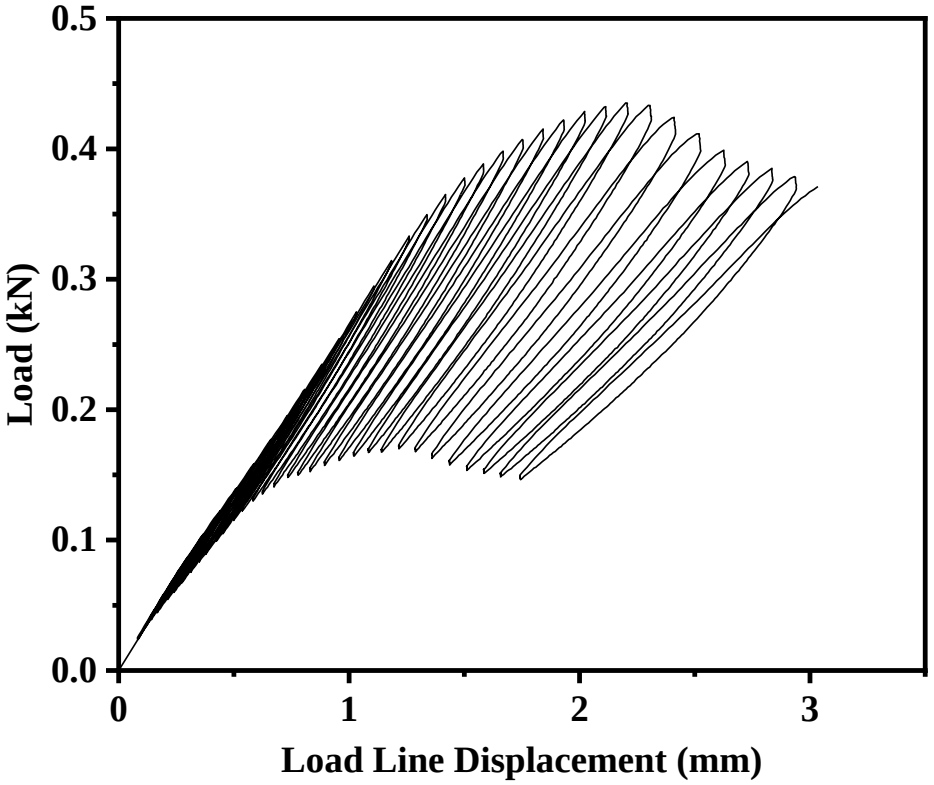

Fig 5.4: Load-Displacement curve of 25% PLA specimen

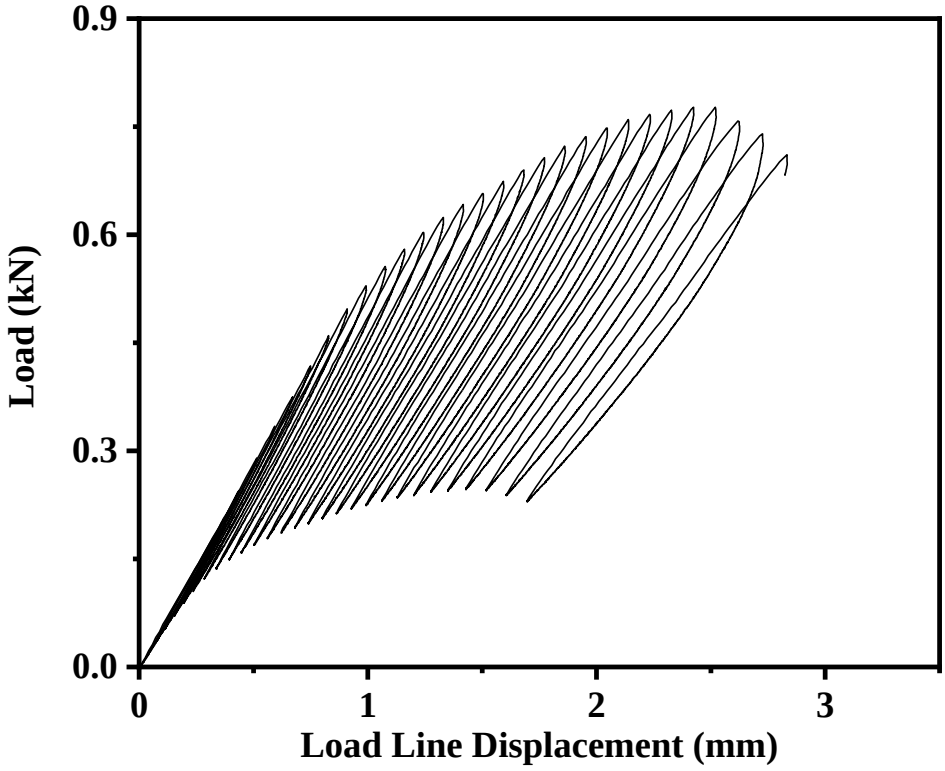

Fig 5.5: Load-Displacement curve of 50% PLA specimen

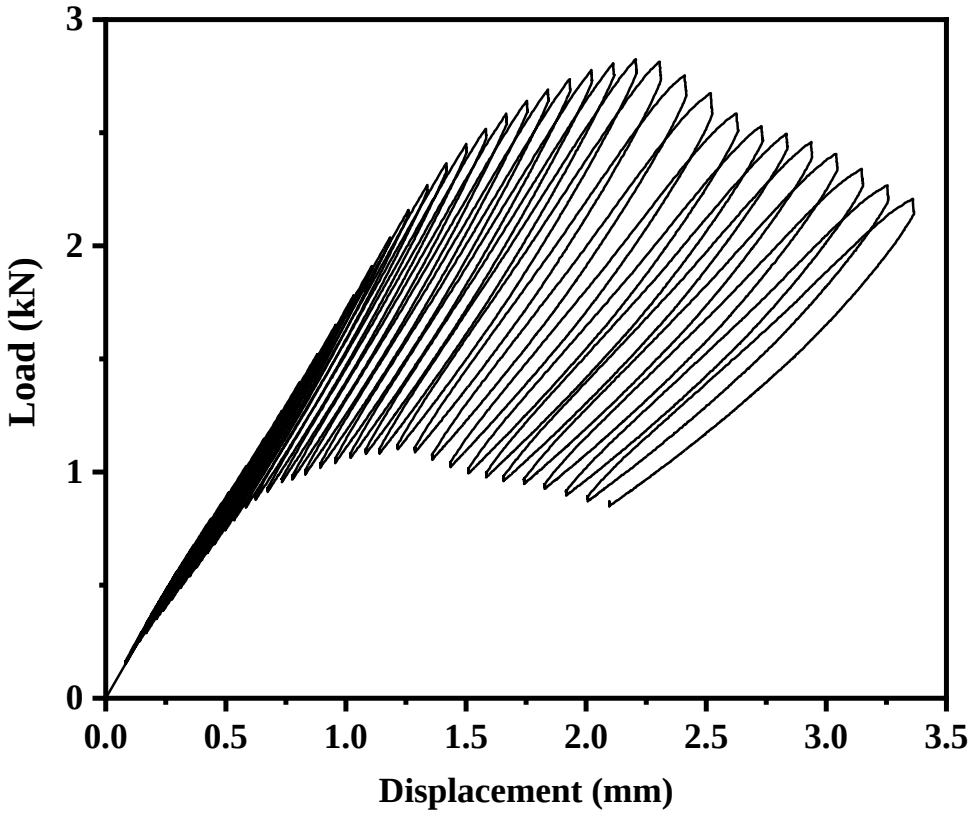

Fig 5.6: Load-Displacement curve of 100% PLA specimen

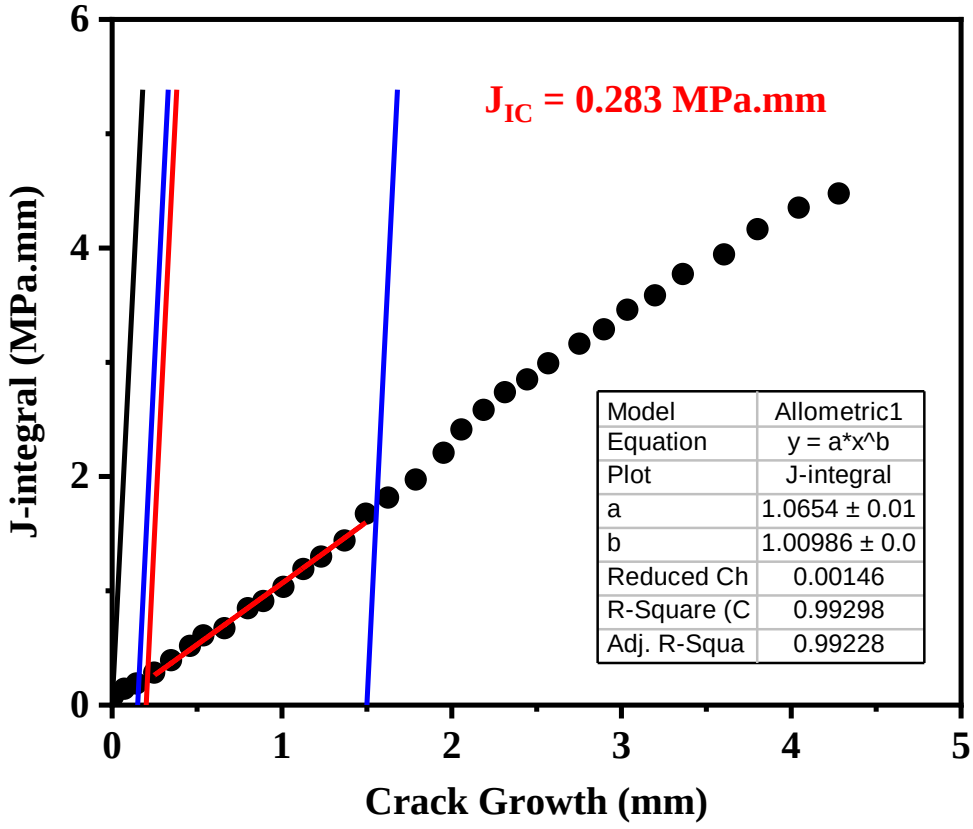

Fig 5.7: J integral vs Crack growth Curve of 25% PLA specimen

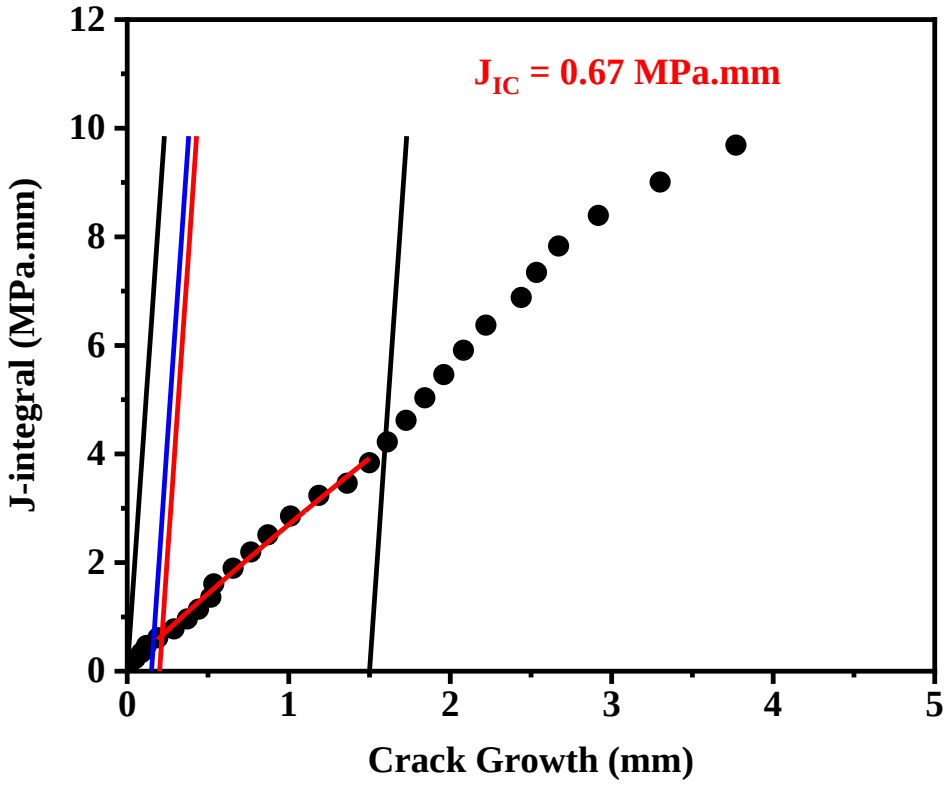

Fig 5.8.: J integral vs Crack growth Curve of 50% PLA specimen

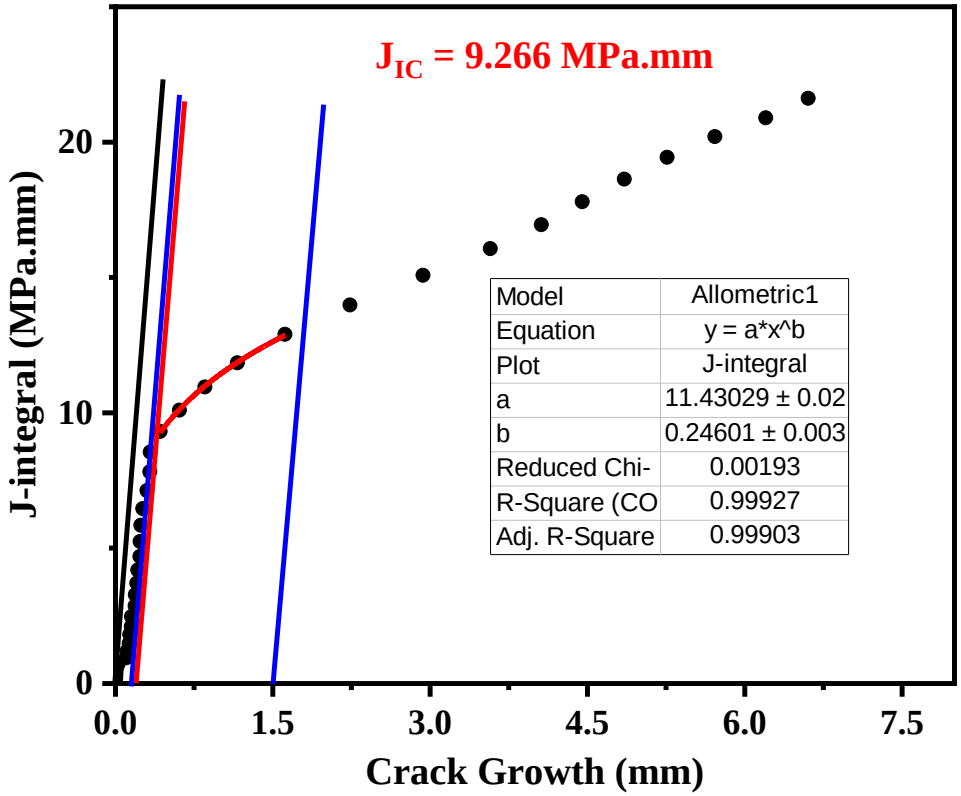

Fig 5.9: J integral vs Crack growth Curve of 100% PLA specimen

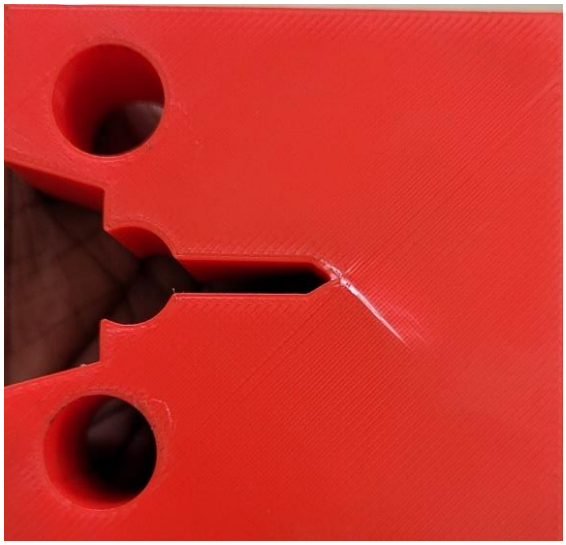

Fig 5.10: Fractured PLA specimen having 100% infill

Table 5.1: Fracture Toughness Test Results

Infill Density (in percentage)	J_{IC} $(MPa.mm)$	Corresponding Young's Modulus from Chapter 3 (GPa)	K_{JC} $(MPa.mm^{0.5})$
25	0.283	0.916	16.10
50	0.67	0.953	25.268
100	9.266	1.253	107.751

5.5 Discussion of results:

The fracture toughness tests conducted on 3D printed PLA specimens having Honeycomb infill pattern with varying infill densities (25%, 50%, and 100%) have yielded valuable insights into the material's fracture behaviour. The J-R curves constructed from the experimental data, along with the calculated J_{IC} and K_{JC} values, provide a quantitative measure of the material's resistance to crack initiation and propagation. The results demonstrate a clear influence of infill density on fracture toughness, with higher infill densities generally exhibiting superior resistance to fracture. The 25% infill density specimen, for instance, displayed a J_{IC}

value of 0.283 MPa.mm and a corresponding KJC of 16.10 $MPa.mm^{0.5}$. The findings of this study underscore the importance of considering infill density as a critical parameter in the design and fabrication of 3D printed PLA components, particularly those subjected to loading conditions that may induce crack formation and growth. By optimizing infill density, engineers and designers can enhance the structural integrity and reliability of 3D printed PLA structures, expanding their potential applications in various fields.

The percentage increase in J_{IC} and K_{JC} values with increasing infill density are as follows:

- **Increase from 25% to 50% infill:**
    - J_{IC}: 136.74% increase
    - K_{JC}: 56.944% increase
- **Increase from 50% to 100% infill:**
    - J_{IC}: 1282.985% increase
    - K_{JC}: 326.471% increase

The observed increase in fracture toughness with higher infill densities can be attributed to several factors:

- **Increased Material Volume:** Higher infill densities result in a greater volume of material within the structure, providing more material to resist crack propagation and absorb energy during fracture.
- **Enhanced Interconnectivity:** Increased infill density leads to improved interconnectivity between the printed layers and filaments, creating a more cohesive and robust structure that is less susceptible to crack initiation and growth.
- **Reduced Void Content:** Higher infill densities reduce the presence of voids and air gaps within the structure, which can act as stress concentrators and promote crack initiation.

- **Improved Load Transfer:** The denser internal structure facilitates better load transfer and distribution throughout the specimen, minimizing localized stress concentrations and reducing the likelihood of crack formation.

5.6 Conclusions:

The study on 3D printed PLA having Honeycomb infill pattern with varying infill densities reveals that higher infill percentages significantly improve fracture toughness. Using Compact Tension (CT) specimens, it was found that 100% infill provided the highest fracture toughness (J_{IC} = 9.266 MPa.mm), indicating superior resistance to crack propagation. This highlights the crucial role of infill density in enhancing the structural integrity of PLA components. The research contributes to understanding fracture mechanics in additive manufacturing, offering valuable insights for optimizing material and process parameters to improve the mechanical performance of 3D printed parts.

Chapter 6: Conclusion and Future scope

6.1 Conclusion:

The thesis comprehensively investigated the mechanical properties of 3D-printed PLA, focusing on the influence of infill density. The key conclusions drawn from the study are as follows:

Tensile Properties: The tensile tests revealed a clear correlation between infill density and mechanical strength. Higher infill densities resulted in increased yield strength, ultimate tensile strength, and Young's modulus. This can be attributed to the greater material volume and improved interconnectivity within the structure at higher infill densities, leading to enhanced load-bearing capacity. The ductility, as measured by percentage elongation, also showed a slight improvement with increasing infill density.

Fatigue Crack Growth Rate (FCGR): The FCGR tests provided valuable insights into the fatigue behaviour of 3D printed PLA. The Paris law parameters (C and m) and the threshold stress intensity factor range (ΔK_{TH}) were determined, enabling the prediction of crack growth rates under cyclic loading conditions. The study highlighted the importance of considering fatigue resistance in the design and application of 3D printed PLA components, especially those subjected to repetitive or fluctuating loads.

Fracture Toughness: The fracture toughness tests demonstrated a significant influence of infill density on the material's resistance to crack initiation and propagation. Higher infill densities led to substantial increases in both the crack initiation fracture toughness (K_{JC}) and the fracture toughness (J_{IC}). This can be attributed to the denser internal structure, reduced void content, and improved load transfer capabilities associated with higher infill densities. The findings emphasize the critical role of infill density in ensuring the structural integrity and reliability of 3D printed PLA components, particularly in applications where crack formation and growth are potential concerns.

Overall Impact: The study's outcomes provide a comprehensive understanding of the mechanical behaviour of 3D printed PLA and its dependence on infill density. The results offer valuable guidance for optimizing the design and fabrication of 3D printed PLA components, enabling engineers and designers to tailor the material's properties to meet specific application requirements. The insights gained from this research contribute to the broader field of additive manufacturing, promoting the wider adoption and utilization of 3D printing technology in various industries.

6.2 Future Scope:

The research conducted in this thesis opens up several avenues for future exploration and advancements in the field of 3D printed PLA and additive manufacturing in general. The following bullet points outline potential future scopes that can build upon the findings and methodologies presented in this work:

- **Exploration of Advanced Infill Patterns and Structures**: The current study focused on a honeycomb infill pattern. Investigating other infill patterns (e.g., gyroid, grid, triangular) and their impact on mechanical properties could provide a more in depth understanding of the connection between a material's composition and its performance in 3D printed PLA. Additionally, exploring the use of functionally graded infill structures, where the infill density varies across different regions of the part, could lead to optimized designs with tailored mechanical performance.
- **Investigation of Other 3D Printing Parameters**: While this research focused on infill density, other factors like layer thickness, nozzle temperature, and printing speed can also greatly impact the strength and durability of 3D-printed PLA. Future study could systematically examine the effects of these variables, both individually and together, to create detailed guidelines for designing 3D-printed PLA parts with the best possible mechanical properties.

- **Multi-Material and Composite 3D Printing**: The incorporation of multiple materials or reinforcing fibres within the 3D printed PLA matrix could lead to the development of advanced composites with enhanced mechanical properties. Future research could explore the feasibility and potential benefits of multi-material and composite 3D printing for PLA, opening up new possibilities for applications requiring high strength, stiffness, or toughness.
- **Long-Term Durability and Environmental Aging**: The current study focused on short-term mechanical testing. Investigating the long-term durability and performance of 3D printed PLA under various environmental conditions (e.g., temperature, humidity, UV exposure) would be crucial for assessing its suitability for long-term applications. Understanding the degradation mechanisms and developing strategies to mitigate them could further enhance the reliability and longevity of 3D printed PLA components.
- **Advanced Characterization Techniques**: Employing advanced characterization techniques such as micro-computed tomography (micro-CT) and scanning electron microscopy (SEM) could provide deeper insights into the microstructure and failure mechanisms of 3D printed PLA. This knowledge could aid in refining the printing process, optimizing material selection, and developing predictive models for mechanical behaviour.
- **Application-Specific Studies**: The current research focused on fundamental mechanical properties. Future studies could investigate the performance of 3D printed PLA in specific applications such as biomedical implants, aerospace components, or automotive parts. This would involve tailoring the material properties and design parameters to meet the specific demands of each application, ensuring optimal functionality and reliability.

- **Comparison of Different 3D Printed Filaments**: The current study focused solely on PLA material. Future research could investigate the mechanical properties (tensile, fatigue, and fracture toughness) of other commonly used 3D printing filaments such as ABS, PETG, Nylon, and TPU. This would allow for a comprehensive comparison of different materials and their suitability for various applications. The influence of infill density on these materials could also be explored to identify optimal printing parameters for each filament type.
- **Comparison of Other Additive Manufacturing Processes**: The present work utilized Fused Deposition Modelling (FDM) as the 3D printing technique. Future studies could extend the investigation to other additive manufacturing processes such as Stereolithography (SLA), Selective Laser Sintering (SLS), and Material Jetting (MJ). Comparing the mechanical properties of PLA parts produced by different AM processes would provide valuable insights into the influence of the manufacturing method on material performance.
- **Hybrid Manufacturing Approaches**: Combining additive manufacturing with traditional manufacturing techniques like injection moulding or machining could lead to the development of hybrid components with unique properties and functionalities. Future research could explore the feasibility and potential benefits of such hybrid approaches for PLA, particularly in applications requiring complex geometries or localized material properties.
- **Optimization of Printing Parameters for Specific Applications**: The current study focused on the general effects of infill density on mechanical properties. Future research could delve deeper into optimizing printing parameters for specific applications, such as biomedical implants, aerospace components, or automotive parts. This would

involve tailoring the material properties and design parameters to meet the specific demands of each application, ensuring optimal functionality and reliability.

- **Development of Predictive Models**: The experimental data generated in this thesis could be used to develop predictive models for the mechanical behaviour of 3D printed PLA. These models could incorporate various factors such as infill density, printing parameters, and loading conditions, enabling engineers and designers to predict the performance of 3D printed PLA components under different scenarios.
- **Investigation of Environmental and Aging Effects**: The long-term durability and performance of 3D printed PLA under various environmental conditions (e.g., temperature, humidity, UV exposure) remain to be fully explored. Future studies could investigate the degradation mechanisms and develop strategies to mitigate them, further enhancing the reliability and longevity of 3D printed PLA components.
- **Exploration of Novel Applications**: The versatility of 3D printed PLA opens up possibilities for its use in various emerging fields such as soft robotics, wearable electronics, and tissue engineering. Future research could focus on developing and characterizing 3D printed PLA structures for these novel applications, pushing the boundaries of additive manufacturing and material science.

By addressing these future research directions, the field of additive manufacturing can continue to evolve and mature, leading to the development of innovative solutions and applications that leverage the unique capabilities of additive manufacturing.

Chapter 7: References

1. Ngo, T. D., Kashani, A., Imbalzano, G., Nguyen, K. T., & Hui, D. (2018). Additive manufacturing (3D printing): A review of materials, methods, applications and challenges. *Composites Part B: Engineering*, *143*, 172-196.
2. Shanmugam, V., Rajendran, D. J. J., Babu, K., Rajendran, S., Veerasimman, A., Marimuthu, U., ... & Ramakrishna, S. (2021). The mechanical testing and performance analysis of polymer-fibre composites prepared through the additive manufacturing. *Polymer testing*, *93*, 106925.
3. Doshi, M., Mahale, A., Singh, S. K., & Deshmukh, S. (2022). Printing parameters and materials affecting mechanical properties of FDM-3D printed Parts: Perspective and prospects. *Materials Today: Proceedings*, *50*, 2269-2275.
4. Samykano, M., Selvamani, SK, Kadirgama, K., Ngui, WK, Kanagaraj, G., & Sudhakar, (2019). Mechanical property of FDM printed ABS: influence of printing parameters. *The International Journal of Advanced Manufacturing Technology*, *102*, 2779-2796.
5. Dawoud, M., Taha, I., & Ebeid, S. J. (2016). Mechanical behaviour of ABS: An experimental study using FDM and injection moulding techniques. *Journal of manufacturing Processes*, *21*, 39-45.
6. Uddin, MS, Sidek, MFR, Faizal, MA, Ghomashchi, R., & Pramanik, A. (2017). Evaluating mechanical properties and failure mechanisms of fused deposition modeling acrylonitrile butadiene styrene parts. *Journal of Manufacturing Science and Engineering*, *139* (8), 081018.
7. Vikneswaran, S. K., Nagarajan, P., Dinesh, S. K., Kumar, K. S., & Megalingam, A. (2022). Investigation of the tensile behaviour of polylactic acid, acrylonitrile butadiene

styrene, and polyethylene terephthalate Glycol materials. *Materials Today: Proceedings*, *66*, 1093-1098.

8. Riddick, J. C., Haile, M. A., Von Wahlde, R., Cole, D. P., Bamiduro, O., & Johnson, T. E. (2016). Fractographic analysis of tensile failure of acrylonitrile-butadiene-styrene fabricated by fused deposition modeling. *Additive Manufacturing*, *11*, 49-59.
9. Musa, L., Kumar, NK, Abd Rahim, SZ, Rasidi, MSM, Rennie, AEW, Rahman, R, & Azmi, AA (2022). A review on the potential of polylactic acid based thermoplastic elastomer as filament material for fused deposition modelling. *journal of materials research and technology*, *20*, 2841-2858.
10. Prajapati, S., Sharma, J. K., Kumar, S., Pandey, S., & Pandey, M. K. (2024). A review on comparison of physical and mechanical properties of PLA, ABS, TPU, and PETG manufactured engineering components by using fused deposition modelling. *Materials Today: Proceedings*.
11. Raney, K., Lani, E., & Kalla, D. K. (2017). Experimental characterization of the tensile strength of ABS parts manufactured by fused deposition modeling process. *Materials Today: Proceedings*, *4*(8), 7956-7961.
12. Arjun, P., Bidhun, V. K., Lenin, U. K., Amritha, V. P., Pazhamannil, R. V., & Govindan, P. (2022). Effects of process parameters and annealing on the tensile strength of 3D printed carbon fiber reinforced polylactic acid. *Materials Today: Proceedings*, *62*, 7379-7384.
13. Mallikarjuna, Balichakra & Mallesh, Vasu & Vardhan, Musunuri & Vadivudaiyanayak, Harshini & Datta, Penjuru. (2024). Effect of Process Parameters on Mechanical Properties in Fused Deposition Modelling of Polyethylene Terephthalate Glycol. Procedia Structural Integrity. 56. 160-166. 10.1016/j.prostr.2024.02.051.

14. Shashikumar, S., & Sreekanth, M.S. (2023). The effect of printing parameters on tensile properties of thermoplastics prepared by fused deposition modeling (FDM) based additive manufacturing technique. *Materials Today: Proceedings*, *90*, 256-261.
15. Zhang, G., Wang, Q., Ni, Y., Liu, P., Liu, F., Leguillon, D., & Xu, LR (2023). A systematic investigation on the minimum tensile strengths and size effects of 3D printing polymers. *Polymer Testing*, *117*, 107845.
16. Rodríguez-Panes, A., Claver, J., & Camacho, A.M. (2018). The influence of manufacturing parameters on the mechanical behavior of PLA and ABS parts manufactured by FDM: A comparative analysis. *Materials*, *11* (8), 1333
17. Akhoundi, B., & Behravesh, A. H. (2019). Effect of filling pattern on the tensile and flexural mechanical properties of FDM 3D printed products. *Experimental Mechanics*, *59*, 883-897.
18. Gao, J., Li, W., Wang, J., Wang, X., Sha, C., & Zhao, K. (2024). Comprehensive analysis of fused deposition modelling process conditions for enhancing mechanical properties and surface quality of 3D-Printed poly-ether-ether-ketone. *Polymer Testing*, *134*, 108432.
19. Ding, S., Zou, B., Wang, P., & Ding, H. (2019). Effects of nozzle temperature and building orientation on mechanical properties and microstructure of PEEK and PEI printed by 3D-FDM. *Polymer Testing*, *78*, 105948.
20. Corapi, D., Morettini, G., Pascoletti, G., & Zitelli, C. (2019). Characterization of a Polylactic acid (PLA) produced by Fused Deposition Modeling (FDM) technology. *Procedia Structural Integrity*, *24*, 289-295.
21. Wang, S., Ma, Y., Deng, Z., Zhang, S., & Cai, J. (2020). Effects of fused deposition modeling process parameters on tensile, dynamic mechanical properties of 3D printed polylactic acid materials. *Polymer testing*, *86*, 106483.

22. Ambruş, S., Muntean, R., Codrean, C., & Uţu, I. D. (2023). Influence of printing conditions on the mechanical properties of copper-polylactic acid composites obtained by 3d printing fused deposition modelling. *Materials Today: Proceedings*, *72*, 580-585.
23. Imran, MA, Singam, KK, Jani, SP, & Uppalapati, S. (2021). Mechanical properties of carbon particle mixed polylactic acid via fused deposition modeling. *Materials Today: Proceedings*, *46*, 8590-8593.
24. Atakok, G., Kam, M., & Koc, HB (2022). Tensile, three-point bending and impact strength of 3D printed parts using PLA and recycled PLA filaments: A statistical investigation. *Journal of Materials Research and Technology*, *18*, 1542-1554.
25. Liu, Z., Lei, Q., & Xing, S. (2019). Mechanical characteristics of wood, ceramic, metal and carbon fiber-based PLA composites manufactured by FDM. *Journal of Materials Research and Technology*, *8* (5), 3741-3751.
26. Vălean, C., Marșavina, L., Mărghitaș, M., Linul, E., Razavi, N., & Berto, F. (2020). Effect of manufacturing parameters on tensile properties of FDM printed specimens. *Procedia Structural Integrity*, *26*, 313-320.
27. Abeykoon, C., Sri-Amphorn, P., & Fernando, A. (2020). Optimization of fused deposition modeling parameters for improved PLA and ABS 3D printed structures. *International Journal of Lightweight Materials and Manufacture*, *3*(3), 284-297.
28. Rao, V. D. P., Rajiv, P., & Geethika, V. N. (2019). Effect of fused deposition modelling (FDM) process parameters on tensile strength of carbon fibre PLA. *Materials Today: Proceedings*, *18*, 2012-2018.
29. Xu, Z., & Razavi, N. (2024). Exploring the impact of thickness, scale and printing sequence on the tensile and fracture properties of PLA specimens fabricated via fused deposition modeling. *Engineering Failure Analysis*, 108587.

30. Ma, Y., Tian, Y., He, Y., Jia, C., Su, B., Shu, X., & Xiao, G. (2024). Characterization of shear/tensile mechanical properties of three-dimensional-printed polylactic acid specimens based on orthogonal raster. *Polymer Testing*, *133*, 108407.
31. Pazhamannil, R. V., Govindan, P., & Sooraj, P. (2021). Prediction of the tensile strength of polylactic acid fused deposition models using artificial neural network technique. *Materials Today: Proceedings*, *46*, 9187-9193.
32. Yadollahi, A., & Shamsaei, N. (2017). Additive manufacturing of fatigue resistant materials: Challenges and opportunities. *International Journal of Fatigue*, *98*, 14-31.
33. Shanmugam, V., Das, O., Babu, K., Marimuthu, U., Veerasimman, A., Johnson, D. J, & Berto, F. (2021). Fatigue behaviour of FDM-3D printed polymers, polymeric composites and architected cellular materials. *International Journal of Fatigue*, *143*, 106007.
34. Sharafi, S., Santare, M. H., Gerdes, J., & Advani, S. G. (2021). A review of factors that influence the fracture toughness of extrusion-based additively manufactured polymer and polymer composites. *Additive Manufacturing*, *38*, 101830.
35. Gardan, J., Makke, A., & Recho, N. (2016). A method to improve the fracture toughness using 3D printing by extrusion deposition. *Procedia Structural Integrity*, *2*, 144-151.
36. He, F., Alshammari, Y.L.A., & Khan, M. (2021). The effect of printing parameters on crack growth rate of FDM ABS cantilever beam under thermo-mechanical loads. *Procedia Structural Integrity*, *34*, 59-64.
37. Azadi, M., Dadashi, A., Dezianian, S., Kianifar, M., Torkaman, S., & Chiyani, M. (2021). High-cycle bending fatigue properties of additive-manufactured ABS and PLA polymers fabricated by fused deposition modeling 3D-printing. *Forces in Mechanics*, *3*, 100016.

38. Khan, T., Ali, M., Riaz, Z., Butt, H., Al-Rub, RKA, Dong, Y., & Umer, R. (2024). Recent developments in improving the fracture toughness of 3D-printed fiber-reinforced polymer composites. *Composites Part B: Engineering*, *283*, 111622.
39. Rezaeian, P., Ayatollahi, M. R., Nabavi-Kivi, A., & Razavi, N. (2022). Effect of printing speed on tensile and fracture behavior of ABS specimens produced by fused deposition modeling. *Engineering Fracture Mechanics*, *266*, 108393.
40. Qu, A., & Li, F. (2023). Effect of double crack on fatigue crack growth life of 3D printing compressor impeller. *Thin-Walled Structures*, *189*, 110883.
41. Ramadas, H., Nath, A. K., Sarkar, S., Ganesh, P., Kaul, R., & Majumdar, J. D. (2022). Fatigue crack growth rate and fracture toughness evaluation of 15-5 precipitation hardening stainless steel fabricated by laser powder bed fusion process. *Materials Science and Engineering: A*, *861*, 144356.
42. Khosravani, M. R., Soltani, P., & Reinicke, T. (2021). Fracture and structural performance of adhesively bonded 3D-printed PETG single lap joints under different printing parameters. *Theoretical and Applied Fracture Mechanics*, *116*, 103087.
43. Leuders, S., Thöne, M., Riemer, A., Niendorf, T., Tröster, T., Richard, H. A., & Maier, H. J. (2013). On the mechanical behaviour of titanium alloy TiAl6V4 manufactured by selective laser melting: Fatigue resistance and crack growth performance. *International journal of fatigue*, *48*, 300-307.
44. Azadi, M., Dadashi, A., Dezianian, S., Kianifar, M., Torkaman, S., & Chiyani, M. (2021). High-cycle bending fatigue properties of additive-manufactured ABS and PLA polymers fabricated by fused deposition modeling 3D-printing. *Forces in Mechanics*, *3*, 100016.
45. Smudde, C. M., D'Elia, C. R., San Marchi, C. W., Hill, M. R., & Gibeling, J. C. (2022). The influence of residual stress on fatigue crack growth rates of additively

manufactured Type 304L stainless steel. *International Journal of Fatigue, 162*, 106954.

46. Daynes, S., Lifton, J., Lu, W. F., Wei, J., & Feih, S. (2021). Fracture toughness characteristics of additively manufactured Ti–6Al–4V lattices. *European Journal of Mechanics-A/Solids*, *86*, 104170.
47. Paul, M.J., Kruzic, J.J., Ramamurty, U., & Gludovatz, B. (2024). The importance of fracture toughness evaluation for additively manufactured metals. *Acta Materialia*, 120061.
48. Dadashi, A., & Azadi, M. (2024). Optimization of 3D printing parameters in polylactic acid bio-metamaterial under cyclic bending loading considering fracture features. *Heliyon* , *10* (4).
49. Senatov, F. S., Niaza, K. V., Stepashkin, A. A., & Kaloshkin, S. D. (2016). Low-cycle fatigue behavior of 3d-printed PLA-based porous scaffolds. *Composites Part B: Engineering*, *97*, 193-200.
50. Vălean, C., Marșavina, L., Mărghitaș, M., Linul, E., Razavi, N., Berto, F., & Brighenti, R. (2020). The effect of crack insertion for FDM printed PLA materials on Mode I and Mode II fracture toughness. *Procedia Structural Integrity, 28*, 1134-1139.
51. Milovanović, A., Milošević, M., Trajković, I., Sedmak, A., Razavi, N., & Berto, F. (2022). Crack path direction in plane-strain fracture toughness assessment tests of quasi-brittle PLA polymer and ductile PLA-X composite. *Procedia Structural Integrity, 42*, 1376-1381.
52. Papon, EA, & Haque, A. (2019). Fracture toughness of additively manufactured carbon fiber reinforced composites. *Additive Manufacturing*, *26*, 41-52.

53. Bakhtiari, H., Nouri, A., & Tolouei-Rad, M. (2024). Impact of 3D printing parameters on static and fatigue properties of polylactic acid (PLA) bone scaffolds. *International Journal of Fatigue*, 108420.

54. Kizhakkinan, U., Rosen, D. W., & Raghavan, N. (2022). Experimental investigation of fracture toughness of fused deposition modeling 3D-printed PLA parts. *Materials Today: Proceedings*, *70*, 631-637.

55. Khosravani, M.R., & Reinicke, T. (2023). Effects of printing parameters on the fracture toughness of 3D-printed polymer parts. *Procedia Structural Integrity*, *47*, 454-459.

56. Shahar, F. S., Sultan, M. T. H., Safri, S. N. A., Jawaid, M., Talib, A. R. A., Basri, A. A., & Shah, A. U. M. (2022). Fatigue and impact properties of 3D printed PLA reinforced with kenaf particles. *Journal of materials research and technology*, *16*, 461-470.

57. Munz, O. J. Photo-Glyph Recording. US Patent 1956, 2, 775,758.

58. Swainson, W. K. Method, Medium and Apparatus for Producing Three-Dimensional Figure Product. US Patent 1977, 4, 041,476.

59. Schwerzel, R. E., et al. Three-Dimensional Photochemical Machining with Lasers. In Applications of Lasers to Industrial Chemistry; Richard, L. Woodin, Andrew, Kaldor, Eds.; SPIE: 1984; pp 90–97.

60. Ciraud, P. A. Process and Device for the Manufacture of any Objects Desired from any Meltable Material. FRG Disclosure Publication 2263777, 1972.

61. The Rapid Prototyping Patent Museum, http://www.additive3d.com/museum/mus_2.html

62. ASTM Committee F42 on Additive Manufacturing Technologies, http://www.astm.org/COMMIT/COMMITTEE/F42.html

63. Wohlers, T. Wohlers Report: Additive Manufacturing State of the Industry. Annual Worldwide Progress Report, 2011, ISBN 0-9754429-6-1
64. 3D Printing in Architecture: One Step Closer to a Sustainable Built Environment - Scientific Figure on ResearchGate. Available from: https://www.researchgate.net/figure/The-range-of-3D-printing-usage-according-to-disciplines-17_fig2_324063338
65. https://standards.iteh.ai/catalog/standards/sist/d9adc3ce-ca51-4c21-b508-00fbbe01687d/iso-astm-52900-2015
66. ASTM D638, 1999 "Standard Test Method for Tensile Properties of Plastics," ASTM International, American Society for Testing and Materials, West Conshohocken, PA, USA.
67. ASTM E647-15a, 2015. "Standard Test Method for Measurement of Fatigue Crack Growth Rates," ASTM International, American Society for Testing and Materials, West Conshohocken, PA, USA.
68. ASTM E1820-13, 2013. "Standard Test Method for Measurement of Fracture Toughness," ASTM International, American Society for Testing and Materials, West Conshohocken, PA, USA.
69. Anderson, Ted L-Fracture mechanics fundamentals and applications, P-332, Chapter 7, Taylor & Francis (2017)
70. Roos, E., 2006. Critical review of the master curve approach with regard to its application in German nuclear power plants. Final report of reactor safety research project no. 1501 240. *MPA Stuttgart*.
71. ASTM E399-12, 2012. "Standard Test Method for Linear-Elastic Plane-Strain Fracture Toughness K_{IC} of Metallic Materials," ASTM International, American Society for Testing and Materials, West Conshohocken, PA, USA.